Available online at www.sciencedirect.com

ScienceDirect

Geochimica et Cosmochimica Acta 139 (2014) 293–312

Geochimica et Cosmochimica Acta

www.elsevier.com/locate/gca

Sources and distributions of branched and isoprenoid tetraether lipids on the Amazon shelf and fan: Implications for the use of GDGT-based proxies in marine sediments

Claudia Zell [a,*], Jung-Hyun Kim [a], David Hollander [b], Laura Lorenzoni [b], Paul Baker [c], Cleverson Guizan Silva [d], Charles Nittrouer [e], Jaap S. Sinninghe Damsté [a]

[a] *NIOZ Royal Netherlands Institute for Sea Research, NL-1790 AB Den Burg, The Netherlands*
[b] *University of South Florida, College of Marine Science, 140 7th Avenue South, St. Petersburg, FL 33701, USA*
[c] *Duke University, Nicolas School of the Environment, 301 Old Chemistry, Box 90227, Durham, NC 27708, USA*
[d] *Departamento de Geologia, Universidade Federal Fluminense, Niterói, RJ, Brazil*
[e] *University of Washington, School of Oceanography, Seattle, WA 98195, USA*

Received 30 September 2013; accepted in revised form 23 April 2014; available online 6 May 2014

Abstract

Branched glycerol dialkyl glycerol tetraethers (brGDGTs) in river fan sediments have been used successfully to reconstruct mean annual air temperature (MAAT) and soil pH of the Congo River drainage basin. However, in a previous study of Amazon deep-sea fan sediments the reconstructed MAATs were ca. 10 °C colder than the actual MAAT of the Amazon basin. In this study we investigated this apparent offset, by comparing the concentrations and distributions of brGDGTs in Amazon River suspended particulate matter (SPM) and sediments to those in marine SPM and surface sediments. The riverine brGDGT input was evident from the elevated brGDGT concentrations in marine SPM and surface sediments close to the river mouth. The distributions of brGDGTs in marine SPM and sediments varied widely, but generally showed a higher relative abundance of methylated and cyclic brGDGTs than those in the river. Since this difference in brGDGT distribution was also found in intact polar lipid (IPL)-derived brGDGTs, which were more recently produced, the change in the marine brGDGT distribution was most likely due to marine in situ production. Consequently, the MAATs calculated based on the methylation of branched tetraethers (MBT) and the cyclisation of branched tetraethers (CBT) were lower and the CBT-derived pH values were higher than those of the Amazon basin. However, SPM and sediments from stations close to the river mouth still showed MBT/CBT values that were similar to those of the river. Therefore, we recommend caution when applying the MBT/CBT proxy, it should only be used in sediment cores that were under high river influence. The influence of riverine derived isoprenoid GDGT (isoGDGT) on the isoGDGT-based TEX_{86} temperature proxy was also examined in marine SPM and sediments. An input of riverine isoGDGTs from the Amazon River was apparent, but its influence on the marine TEX_{86} was minor since the TEX_{86} of SPM in the Amazon River was similar to that in the marine SPM and sediments.

* Corresponding author. Address: Professur für Biogeowissenschaften ETH Zürich Sonneggstrasse 5. Tel.: +41 44 632 36 66; fax: +31 0 222 319674.
E-mail address: claudia.zell@nioz.nl (C. Zell).

http://dx.doi.org/10.1016/j.gca.2014.04.038
0016-7037/

1. INTRODUCTION

During the last decade, the implementation of high-performance liquid chromatography/mass spectrometry (HPLC/MS) has enabled the detection of structurally diverse intact glycerol dialkyl glycerol tetraethers (GDGTs) (see Schouten et al., 2013a,b for a review). The most commonly detected tetraether lipids in coastal marine sediments are branched and isoprenoid GDGTs (brGDGTs and isoGDGTs, respectively).

BrGDGTs are membrane-spanning lipids most likely of anaerobic (e.g. Weijers et al., 2006a,b) and heterotrophic (Pancost and Sinninghe Damsté, 2003; Oppermann et al., 2010) bacteria that are ubiquitous in peat (Weijers et al., 2006a) and soil (Weijers et al., 2007b). Recent studies indicate that some acidobacterial species produce brGDGT-Ia (Fig. 1) (Weijers et al., 2009a; Sinninghe Damsté et al., 2011), but the producers of other brGDGTs remain unknown. The brGDGTs vary in the degree of methylation (4–6) and may contain up to two cyclopentane moieties formed by internal cyclization (Sinninghe Damsté et al., 2000; Weijers et al., 2006a) (Fig. 1). The distribution of the brGDGTs in soils, as expressed by the degree of methylation (methylation index of branched tetraethers; MBT) and cyclization (cyclization index of branched tetraethers; CBT) of the brGDGTs, correlates with mean annual air temperature (MAAT) and soil pH (Weijers et al., 2007b; Peterse et al., 2012). Hence, the MBT/CBT proxy has been used to reconstruct past environmental and climate changes in diverse settings: marine (e.g. Weijers et al., 2007b; Donders et al., 2009; Rueda et al., 2009; Bendle et al., 2010), and lacustrine (e.g. Tyler et al., 2010; Zink et al., 2010; Fawcett et al., 2011) sediments, peat (Ballantyne et al., 2010), and loess (Peterse et al., 2011b). Weijers et al. (2007a) applied the MBT/CBT proxy in Congo deep-sea fan sediments, assuming that brGDGTs were mainly produced in soils, washed into small streams and rivers by soil erosion, and further transported to the ocean. Since then it has been argued that the MBT/CBT paleothermometer of deep-sea fan sediments reflect an integrated environmental signal of the whole river basin. However, it has also been found that the brGDGT distributions in marine sediments might be altered by in situ production and degradation processes in the marine environment (Peterse et al., 2009; Zhu et al., 2011; Hu et al., 2012).

Following the successful use of the MBT/CBT proxy in the Congo deep-sea fan, Bendle et al. (2010) in turn applied it to the Amazon deep-sea fan sediments. In contrast to the findings of Weijers et al. (2007a), the reconstructed MAAT in the Amazon decreased from the glacial period (20–23 °C) to the mid-Holocene (~10 °C), increasing over the remainder of the Holocene to 17 °C. It was postulated that an increased brGDGT contribution from the Andes region was responsible for the observed decrease of the reconstructed MAAT during the Holocene (Bendle et al., 2010). However, subsequent studies (Kim et al., 2012b; Zell et al., 2013a) have shown that the brGDGTs in the river suspended particulate matter (SPM) and riverbed sediments in the central Amazon basin do not predominantly originate from the high Andes soils (>2500 m in altitude). Zell et al. (2013a) found that the MBT/CBT-derived temperature from the lower Amazon River was about 2 °C lower than that in surrounding soils. This difference was related to in situ production in the river and highlights the complex interplay between allochthonous and autochthonous sources of brGDGTs. However, this can also only

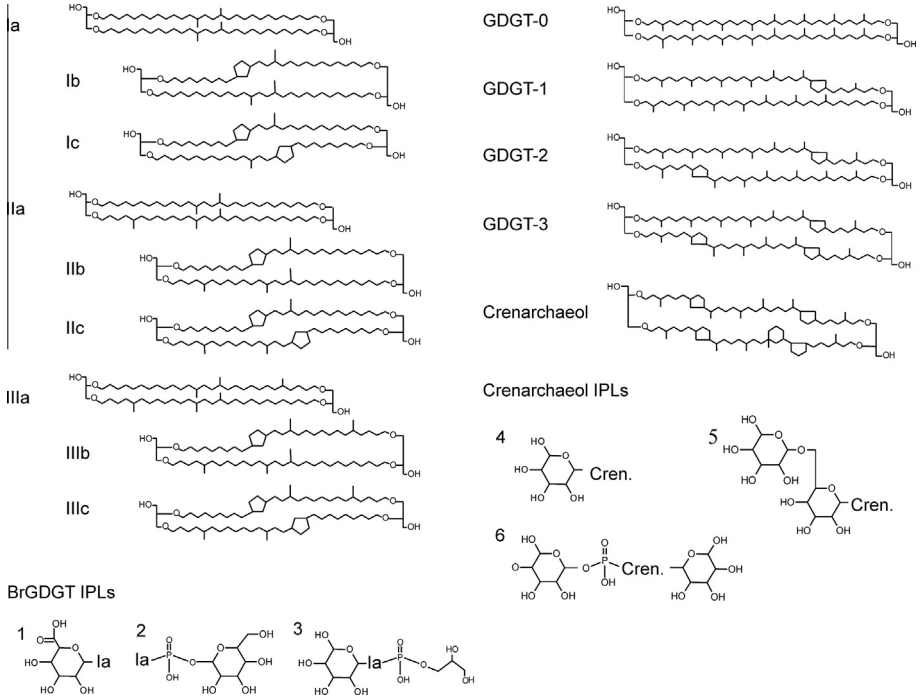

Fig. 1. Chemical structures of brGDGTs (Ia–IIIc) and isoGDGTs (GDGT-0–GDGT-3 and crenarchaeol) and the detected IPLs of brGDGT Ia and crenarchaeol in this study (1-6).

partially explain the ~10 °C lower estimates of Holocene temperatures in Amazon deep-sea fan sediments (Bendle et al., 2010). In order to understand why the MBT/CBT can be used to reconstruct the climate of the Congo basin, but shows obvious problems in the reconstruction of the Amazon basin climate, a detailed study of sources of brGDGTs in marine sediments under the influence of the Amazon River is required.

IsoGDGTs are membrane-spanning lipids mainly biosynthesized by Thaumarchaeota, formerly known as Group I Crenarchaeota (Brochier-Armanet et al., 2008; Spang et al., 2010). They are abundant in both marine environments (e.g. Schouten et al., 2002; Kim et al., 2010) and lakes (e.g. Blaga et al., 2009; Sinninghe Damsté et al., 2009; Powers et al., 2010). There occur isoGDGTs containing 0–4 cyclopentane moieties, and there is crenarchaeol and its regio-isomer, which in addition to 4 cyclopentane moieties contain a cyclohexane moiety (Schouten et al., 2000, 2008; Sinninghe Damsté et al., 2002) (Fig. 1). Schouten et al. (2002) found that the number of cyclopentane moieties in marine sediments increased with increasing sea surface temperature (SST) and thus introduced the TEX_{86} (TetraEther indeX of tetraethers consisting of 86 carbon atoms) as a SST proxy. More recently, the TEX_{86} was refined as TEX_{86}^{H} for tropical and subtropical oceans (Kim et al., 2010), and a new water-depth-integrated annual mean temperature calibration (0–200 m water depth) has been introduced (Kim et al., 2012b). Since isoGDGTs also occur in soil (Weijers et al., 2006b) and river SPM (e.g. Herfort et al., 2006; Kim et al., 2007) the distribution of isoGDGTs in marine sediments can be influenced by input of riverine isoGDGTs (Weijers et al., 2006b), presumably affecting the TEX_{86}^{H} proxy inference.

In this study, we compared the concentrations and distributions of brGDGTs and isoGDGTs in the Amazon shelf and deep-sea fan with those in the adjacent terrestrial Amazon basin in order to assess the impact of the brGDGT provenance on the application of the MBT/CBT proxy in this region. Since brGDGTs have been extensively studied in soils and SPM in the Amazon basin (Kim et al., 2012a,b; Zell et al., 2013a,b) the present study is fully focused on the potential sources of both brGDGTs and isoGDGTs in the marine environment. This is an essential step in order to be able to confidently apply the MBT/CBT, BIT and TEX_{86}^{H} proxies to marine sediment cores. To identify sources of the GDGTs, we examined the presence of reported intact polar lipids (IPLs) of brGDGTs and crenarchaeol (Liu et al., 2010; Pitcher et al., 2010, 2011; Peterse et al., 2011a) as well as the concentrations and distributions of IPL-derived GDGTs as in the approach by Zell et al. (2013a,b). This study provides new insights on the interpretation of the GDGT-based sedimentary record of the Amazon River deep-sea fan and for other river systems.

2. STUDY AREA: THE AMAZON SHELF AND FAN

The Amazon River (Fig. 2A) is the largest drainage system in the world in terms of fresh-water discharge (Milliman and Meade, 1983) and catchment area (Goulding et al., 2003). The mean annual water discharge is 2×10^5 m^3 s^{-1} at Óbidos, the most downstream gauging station in the Amazon River (Callède et al., 2000). The Amazon River ranks second globally in terms of suspended sediment particle transport, with an annual mean sediment discharge of $8–12 \times 10^{11}$ kg y^{-1} at Óbidos (Dunne et al., 1998). Once on the Amazon Shelf, the Amazon River plume is advected offshore and transported northwestward along the north Brazilian coast as it is entrained by the North Brazilian Current, covering most of the continental shelf from 1°S to 5°N (Muller-Karger et al., 1988). Average annual water temperature and salinity provides an idea about the extent of the Amazon River plume (Fig. 2B and C). Over the shelf, the Amazon freshwater plume is typically 3–10 m thick and between 80–200 km wide (Fig. 2C; Lentz and Limeburner, 1995). The Amazon shelf is strongly influenced by tidal currents with an extreme tidal range of 10 m at the mouth of the Amazon River (Gibbs, 1982). The flow of the Amazon River is so large that the estuary effectively extends across the entire inner shelf, in a band within 25 km off the river mouth. The estuarine-like circulation on the shelf allows high-salinity ocean water to penetrate underneath the low-salinity surface plume and prevents most riverine sediments from escaping off the shelf, causing a sediment deposition as a band of highly mobile, inner shelf muds extending 1600 km north-west and 50–150 km across the shelf (Nittrouer and DeMaster, 1986). Thus, the Amazon shelf is an area of active sediment deposition at an estimated rate of $\sim 6 \times 10^{11}$ kg y^{-1} (Kuehl et al., 1986).

The Amazon fan (or Amazon cone) is globally the third largest modern 'mud-rich' deep-sea fan and forms a significant proportion of the continental margin of Brazil (Damuth and Flood, 1985). The Amazon Fan extends downslope from the shelf break for ~700 km and exhibits an elongated radial pattern covering $\sim 3.3 \times 10^5$ km^2. When sea-level was low during glacial periods, sediment eroded from the continent within the Amazon drainage basin was transported directly to the fan (Damuth and Kumar, 1975). In contrast, when sea-level was high during interglacial periods (such as today), the sediment load from the river was transported in long shore currents to the northwest and deposited on the continental shelf (Milliman et al., 1975; Nittrouer and DeMaster, 1986).

3. MATERIALS AND METHODS

3.1. Sample collection

Marine SPM and surface sediments over the Amazon Shelf and slope were collected on board of the R/V Knorr 197-4 between February and March 2010 (Table 1). Sediment was collected at all stations, but SPM was only collected along the sampling stations of the two transects as indicated in Fig. 2D. SPM sampling was carried out at two water depths, at the chlorophyll maximum (chl_{max}) and close to the bottom. The depth of the chl_{max} was determined with a fluorescence detector (Fluorescence, Wetlab ECO-AFL/FL). The water used to determine the SPM concentration and the total organic carbon (TOC)

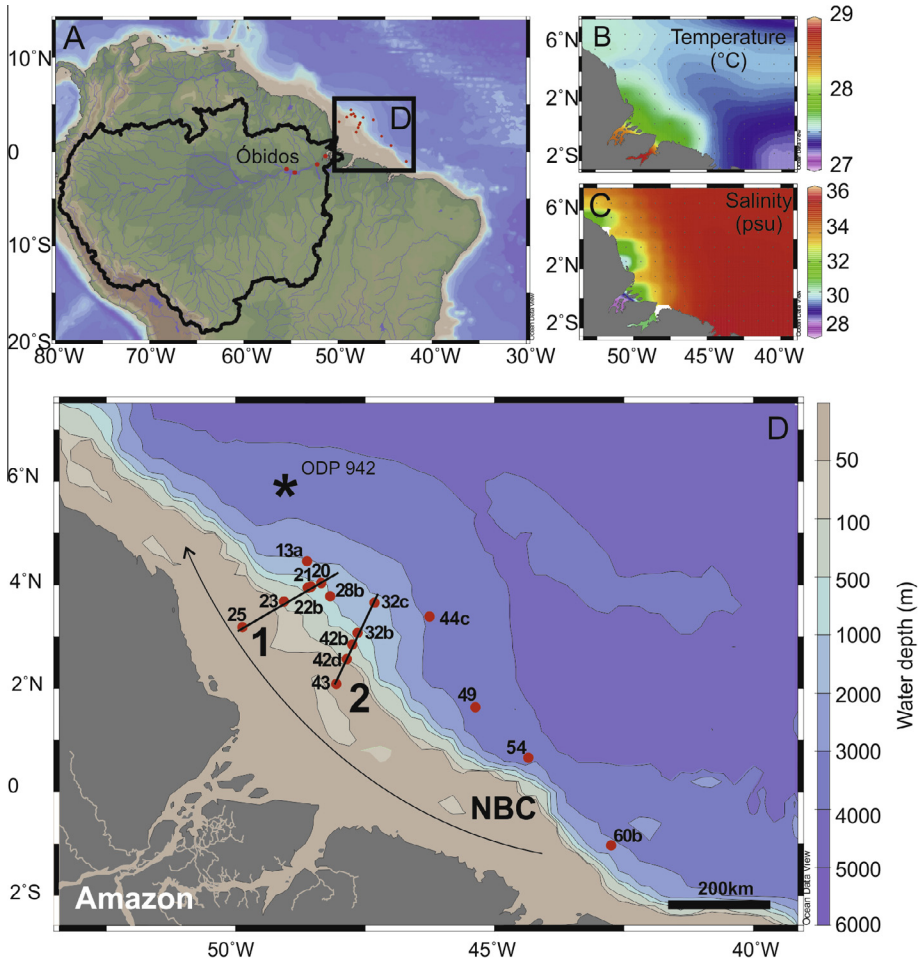

Fig. 2. (A) Map of the Amazon basin showing the Amazon watershed (back line) and the sampling stations (red dots). (B) Mean annual SST and (C) mean annual salinity in the western tropical Atlantic from the world ocean atlas 09 (WOA09) data set (Antonov et al., 2010; Locarnini et al., 2010). (D) Detailed view of the marine study area showing the sampling stations and indicating transects 1 and 2. NBC = North Brazilian Current.

analysis of the SPM was collected with Niskin bottles. Between 1 and 26 L of this water were filtered onto ashed (450 °C, overnight) and pre-weighed glass fibre filters (Whatman GF-F, 0.7 μm, 47 mm diameter). For the lipid analysis about 300 L of water were separately filtered onto ashed glass fibre filters with in situ pumps (Whatman GF-F, 0.7 μm, 142 mm diameter, WTS, McLane Labs, Falmouth, MA). All samples were kept frozen at −20 °C and freeze dried before analysis. Sediment cores were collected using a box corer from which the top 1 cm was subsampled.

River SPM was taken at Óbidos, which is the last gauging station in the Amazon River and located 800 km westwards from the Atlantic Ocean just beyond tidal influences. Four SPM samples were collected each of them at a different river water level: rising, high, falling and low water level (Zell et al., 2013b). In addition, three river-bed sediments were collected in 2010; one 26 km downstream from Óbidos and the other two close to the Amazon River mouth (Fig. 2A).

3.2. Environmental parameter and bulk geochemical analysis

The pH of the sediment samples was measured in a mixture of sediment and distilled water 1:3.5 (v:v). This water and sediment were stirred vigorously and left to settle for 20 min. The pH was measured with a Wissenschaftlich-Technische Werkstätten pH 315i/SET and probe pH-Electrode SenTix 41 (pH 0–14, T 0–80 °C, stored in 3 mol L^{-1} KCl) at the Netherlands Institute for Sea Research (NIOZ). Before the pH measurements, the pH analyzer was calibrated with CertiPUR buffer solutions with pH 4.01, 7.00, and 10.00.

All sediment samples were freeze dried and decarbonated (using 2 mol L^{-1} HCl) prior to analyses. The marine SPM filters were also decarbonated using HCl vapor as described by Lorrain et al. (2003). The TOC contents of the marine sediments were analyzed with a Fison NA 1500 Elemental Analyzer at the University of South Florida (USF, USA). The analyses were determined in duplicates and the precision was 0.1 mg OC g^{-1}. Particulate organic

Table 1
Amazon River and marine SPM and sediment samples studied and their general properties.

	Sampling date (dd/mm/yy)	Longitude	Latitude	Sampling water depth (m)	CTD water temperature (°C)	Annual mean temperature 0–200 m (°C)[b]	Measured pH	OC (wt.%)
Amazon River SPM								
CBM5 (high water)	03/07/09	55.47	1.97	Surface	28.8	–	6.2	3.0
CBM6 (low water)	16/10/09	55.49	1.95	Surface	31.0	–	6.8	3.3
CBM7 (falling water)	08/09/10	55.50	1.95	Surface	30.5	–	7.0	3.0
CBM8 (rising water)	01/02/11	55.55	1.91	Surface	28.7	–	6.8	1.0
Amazon River sediments								
AMAZA 26	–[a]	−54.25	−2.41	–	–	–	–	0.6
AMAZC RO11B	–	−51.01	−0.13	–	–	–	–	0.2
AMAZC RO3	–	−50.80	−0.95	–	–	–	–	0.6
Marine SPM								
13a	23/02/10	−48.61	4.46	1700	4.0	23.1	–	0.5
13a	23/02/10	−48.61	4.46	85	27.2	23.1	–	0.9
20	24/02/10	−48.35	4.04	1000	5.0	23.1	–	2.0
20	24/02/10	−48.35	4.04	75	27.5	23.1	–	5.2
21	25/02/10	−48.54	3.96	700	5.4	23.1	–	0.6
21	25/02/10	−48.54	3.96	85	27.8	23.1	–	6.0
22b	25/02/10	−48.61	3.95	600	5.9	23.1	–	2.8
22b	25/02/10	−48.61	3.95	89	27.7	23.1	–	16.3
23	25/02/10	−49.06	3.68	100	24.0	23.4	–	10.0
23	25/02/10	−49.06	3.68	75	27.9	23.4	–	13.7
25	26/02/10	−49.86	3.19	25	27.5	27.6	–	0.6
25	26/02/10	−49.86	3.19	5	28.7	27.6	–	4.3
28b	27/02/10	−48.17	3.78	990	5.0	23.1	–	0.6
28b	27/02/10	−48.17	3.78	100	27.4	23.1	–	0.5
32b	28/02/10	−47.64	3.07	1777	3.9	23.2	–	0.8
32b	28/02/10	−47.64	3.07	100	26.3	23.2	–	1.4
42b	02/03/10	−47.74	2.85	590	6.2	23.4	–	0.7
42b	02/03/10	−47.74	2.85	90	27.0	23.4	–	1.4
42c/d	03/03/10	−47.85	2.57	200	12.1	23.4	–	2.1
42c/d	03/03/10	−47.85	2.57	60	26.4	23.4	–	0.9
42d	03/03/10	−47.85	2.57	100	24.7	23.4	–	0.2
42d	03/03/10	−47.85	2.57	60	26.9	23.4	–	0.8
43	03/03/10	−48.05	2.09	55	27.5	26.7	–	0.7
43	03/03/10	−48.05	2.09	10	28.3	26.7	–	0.9
Marine surface sediments								
13a	23/02/10	−48.61	4.46	1711	–	23.1	7.9	0.9
20	24/02/10	−48.35	4.04	1088	–	23.1	7.9	1.1
21	25/02/10	−48.54	3.96	738	–	23.1	8.0	1.1
22b	25/02/10	−48.61	3.95	640	–	23.1	8.0	0.7
23	25/02/10	−49.06	3.68	107	–	23.4[c]	8.0	0.6
25	26/02/10	−49.86	3.19	32	–	27.6[c]	8.2	0.7
28b	27/02/10	−48.17	3.78	1014	–	23.1	8.0	1.0
32b (=42a)	28/02/10	−47.64	3.07	1028	–	23.2	7.9	0.7
32c	02/03/10	−47.31	3.65	2079	–	23.4	8.0	1.1
42b	02/03/10	−47.74	2.85	609	–	23.4	8.0	0.8
42d	03/03/10	−47.85	2.57	110	–	23.4[c]	9.0	0.1
43	03/03/10	−48.05	2.09	65	–	26.7[c]	8.9	0.0
44c	04/03/10	−46.25	3.39	3375	–	22.9	7.9	1.1
49	04/03/10	−45.36	1.64	–	–	22.8	8.1	1.4
54	07/03/10	−44.35	0.66	2372	–	23.1	8.1	0.3
60b	10/03/10	−42.74	−1.03	3113	–	23.2	7.9	1.0

[a] '–' = no data available.
[b] Data from the world ocean atlas 09 (WOA09) data set (Locarnini et al., 2010).
[c] Depth integrated temperature for 0–100 m water depth.

carbon (POC) and TOC of Amazon River sediment were analyzed with a Thermo-Scientific Flash 2000 Elemental Analyzer at the NIOZ. The analyses were determined in duplicate and the precision was 0.2 mg OC g^{-1}.

3.3. Extraction and analysis of GDGTs

Extraction and analysis of core lipid (CL), IPL-derived GDGTs and IPLs were carried out in the same way as described by Zell et al. (2013a,b). Briefly, the freeze-dried samples were extracted with a modified Bligh and Dyer technique (Pitcher et al., 2009) and fractioned into CLs and IPLs (Oba et al., 2006; Pitcher et al., 2009). For GDGT quantification, 0.1 mg C_{46} GDGT internal standard was added (Huguet et al., 2006). Part of the IPL fraction was hydrolyzed to obtain IPL-derived CLs (Weijers et al., 2011). The CL GDGTs were analyzed using high performance liquid chromatography atmospheric pressure positive ion chemical ionization–mass spectrometry in selected ion monitoring mode (Schouten et al., 2007).

For the analysis of IPLs in SPM samples and marine sediments four sampling stations (25, 28b, 42d, and 43, see Fig. 2D) were chosen. To analyze the brGDGT IPLs a selective reaction monitoring (SRM) method according to Peterse et al. (2011a,b) was used. Crenarchaeol IPLs were detected by high-performance liquid chromatography–electrospray ionization–tandem mass spectrometry using an SRM method (Pitcher et al., 2011).

3.4. Calculation of GDGT-based indices

In the following equations, the numerals refer to the GDGTs indicated in Fig. 1. The BIT (Branched and Isoprenoid Tetraether) index (Hopmans et al., 2004), the degree of cyclization (DC, Sinninghe Damsté et al., 2009), and the MBT and CBT values (Weijers et al., 2007b) were calculated as follows:

$$\text{BIT index} = \frac{[\text{Ia}] + [\text{IIa}] + [\text{IIIa}]}{[\text{Ia}] + [\text{IIa}] + [\text{IIIa}] + [\text{IV}]} \quad (1)$$

$$\text{DC} = \frac{[\text{Ib}] + [\text{IIb}]}{[\text{Ia}] + [\text{Ib}] + [\text{IIa}] + [\text{IIb}]} \quad (2)$$

$$\text{CBT} = -\log\left(\frac{[\text{Ib}] + [\text{IIb}]}{[\text{Ia}] + [\text{IIa}]}\right) \quad (3)$$

$$\text{MBT} = \frac{[\text{Ia}] + [\text{Ib}] + [\text{Ic}]}{[\text{Ia}] + [\text{Ib}] + [\text{Ic}] + [\text{IIa}] + [\text{IIb}] + [\text{IIc}] + [\text{IIIa}] + [\text{IIIb}] + [\text{IIIc}]} \quad (4)$$

For the calculation of pH and temperature, the regional soil calibration for the Amazon basin was used (Bendle et al., 2010):

$$\text{CBT} = 4.23 - 0.58 \times \text{pH} \ (r^2 = 0.75, n = 37) \quad (5)$$

$$\text{MBT} = 0.19 + 0.08 \times \text{CBT} + 0.03 \times \text{MAAT} \ (r^2 = 0.91, n = 37) \quad (6)$$

TEX_{86} was calculated according to Schouten et al. (2002). The TEX_{86} values were converted to temperatures using the global core-top calibrations for 0–200 m water depth (Kim et al., 2012b):

$$\text{TEX}_{86} = \frac{[\text{GDGT}-2] + [\text{GDGT}-3] + [\text{Cren}']}{[\text{GDGT}-1] + [\text{GDGT}-2] + [\text{GDGT}-3] + [\text{Cren}']} \quad (7)$$

$$\text{T}(^{\circ}\text{C}) = 54.7 \times \log(\text{TEX}_{86}) + 30.7 \ (r^2 = 0.84, n = 255, p < 0.0001) \quad (8)$$

4. RESULTS

4.1. Amazon river SPM and sediments

The concentrations of brGDGTs in river SPM varied between 30 and 100 μg g_{OC}^{-1} (30 and 100 brGDGT ng L^{-1}) for the CL fraction and between 2 and 16 μg g_{OC}^{-1} (2 and 18 brGDGT ng L^{-1}) for the IPL fraction (Fig. 3A and B; Table 2). The IPL fraction was on average 12% of the total amount of brGDGTs. In the river-bed sediments, the concentrations of CL brGDGTs were between 60 and 170 μg g_{OC}^{-1}, while the concentrations of IPL-derived brGDGTs were between 4 and 17 μg g_{OC}^{-1} (Table 2), which is on average 7% of the total amount of brGDGTs. The distribution of brGDGTs in river SPM and sediments were similar (Fig. 4A). The most abundant brGDGT in both river SPM and sediments was brGDGT Ia, with an average of 75% and 72% of the total CL brGDGTs and the total IPL-derived brGDGTs, respectively. The MBT values of the river SPM and sediments varied between 0.80 and 0.86 in the CL brGDGTs, and between 0.77 and 0.09 in the IPL-derived brGDGTs (Fig. 5A). The DC values of river SPM and sediments were 0.06–0.11 in the CL brGDGTs and 0.05–0.13 in the IPL-derived brGDGTs (Fig. 5B). The CBT-derived pH of CL brGDGTs varied from 5.3 to 5.7 and from 5.1 to 5.9 in the IPL fraction (Fig. 5C). The MBT/CBT-derived MAAT ranged from 21 to 24 °C in the CL brGDGTs and from 21 to 24 °C in the IPL-derived brGDGTs (Fig. 5D).

The concentrations of isoGDGTs of river SPM were 34–99 μg g_{OC}^{-1} (27–76 ng L^{-1}) for the CL fraction and 5–15 μg g_{OC}^{-1} (4–11 ng L^{-1}) for the IPL fraction (Fig. 3C and D, Table 2). IPL-derived isoGDGTs represented on average 32% of the total amount of isoGDGTs. River sediments contained 20–54 μg g_{OC}^{-1} of CL isoGDGTs and 13–30 μg g_{OC}^{-1} of IPL-derived isoGDGTs (Table 2). IPL-derived isoGDGTs represented on average 40% of the total isoGDGTs. In the CL fraction of SPM the most dominant isoGDGT was crenarchaeol (Fig. 6A), representing 55% of all isoGDGTs. In the sediments GDGT-0 was the most common isoGDGT (51%) (Fig. 6A). GDGT-0 was also the most common isoGDGT in the IPL fraction of river SPM and sediments, representing 40% and 71% of all isoGDGTs, respectively. This results in a GDGT-0 to crenarchaeol ratio in river SPM and sediments varying between 0.2 and 2.3 in the CL isoGDGTs and between 1.0 and 12.6 in the IPL-derived isoGDGTs (Fig. 7A). The TEX_{86} values of CL and IPL-derived isoGDGTs were

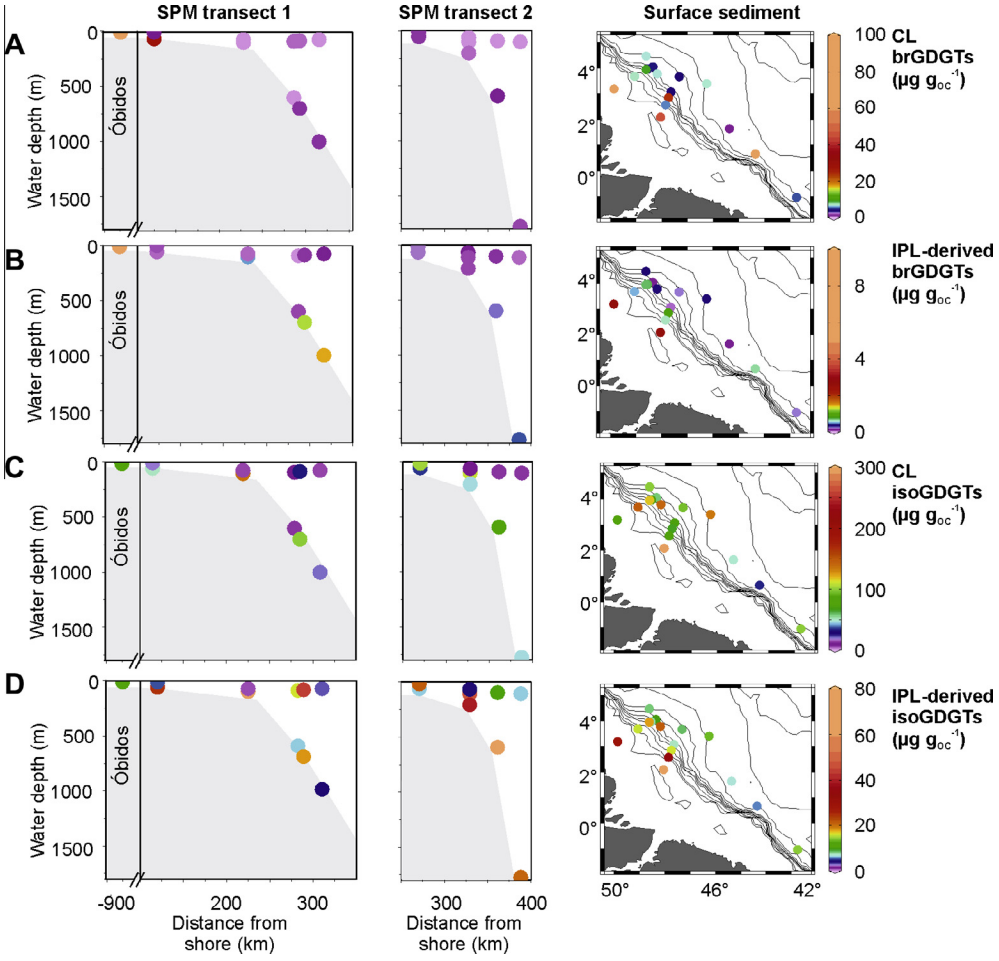

Fig. 3. CL and IPL-derived brGDGT concentrations (A, B) and CL and IPL-derived isoGDGT concentrations (C, D) in riverine and marine SPM (transects 1 and 2; see Fig. 2D) and in marine surface sediments.

0.64–0.74 and 0.66–0.83, respectively (Fig. 7B). The TEX_{86}-derived temperatures were 21–30 °C for CL isoGDGTs and 29–32 °C for IPL-derived isoGDGTs (Fig. 7C). The BIT of river SPM was between 0.4 and 0.9 in the CL fraction and between 0.3 and 0.7 in the IPL fraction (Fig. 7D), while the river sediments had an average BIT of 0.9 in the CL fraction and of 0.7 in the IPL fraction.

4.2. Marine SPM

From the sampling station closest to the river mouth (station 25; Fig. 2D), the brGDGT concentration in marine SPM decreased rapidly. In the bottom water SPM of station 25, the concentration of the CL brGDGTs was 28 µg g_{OC}^{-1} (2 µg L^{-1}), while the concentration of the IPL-derived brGDGTs was 0.1 µg g_{OC}^{-1} (0.3 µg L^{-1}) (Fig. 3A and B, Table 2), comprising 0.3% of the total brGDGTs. At all other stations, the concentrations of the brGDGTs varied between 0 and 2 µg g_{OC}^{-1} (0–0.02 µg L^{-1}) for the CL fraction and 0 and 1.4 µg g_{OC}^{-1} (0–0.02 µg L^{-1}) for the IPL fraction, which comprised (Fig. 3A and B; Table 2), on average, 43% of the total amount of brGDGTs present. As in the river SPM, brGDGT Ia was the most abundant brGDGT in marine SPM (Fig. 4B). However, relative abundance of brGDGT Ia in the marine SPM was more variable than in the river, accounting for 30–100% of the total amount of the detected CL brGDGTs. MBT and DC could not be calculated for some of the SPM samples, as there was not sufficient material to detect all the brGDGTs required to calculate these indexes. This was especially the case for SPM from the chl_{max} (Table 2). For the samples in which the MBT and CBT were calculated, the MBT ranged from 0.28 to 0.94 in the CL brGDGTs, and from 0.77 to 0.96 in the IPL-derived brGDGTs (Fig. 5A). The DC varied between 0.03 and 0.38 in the CL fraction and between 0.03 and 0.4 in the IPL fraction (Fig. 5B). The CBT-derived pH varied from 4.6 to 8.3 in the CL brGDGTs and from 4.6 to 8.4 in the IPL-derived brGDGTs (Fig. 5C). The MBT/CBT-derived MAAT ranged from 17 to 28 °C in the Cl brGDGTs and from 23 to 29 °C in the IPL-derived brGDGTs (Fig. 5D).

The concentrations of CL isoGDGTs in marine SPM ranged from 3 to 160 µg g_{OC}^{-1} and those of the IPL-derived isoGDGTs from 1.8 to 82 µg g_{OC}^{-1} (Fig. 3C, D, Table 2). IPL-derived isoGDGTs comprised on average 34% of the total amount of isoGDGTs. The concentrations were in

Table 2
Concentrations of brGDGTs and isoGDGTs normalized to OC.

	brGDGTs																		isoGDGTs[b]											
	CL ($\mu g\ g_{OC}^{-1}$)									IPL-derived ($\mu g\ g_{OC}^{-1}$)									CL ($\mu g\ g_{OC}^{-1}$)						IPL-derived ($\mu g\ g_{OC}^{-1}$)					
	Ia	Ib	Ic	IIa	IIb	IIc	IIIa	IIIb	IIIc	Ia	Ib	Ic	IIa	IIb	IIc	IIIa	IIIb	IIIc	0	1	2	3	Cren	Cren'	0	1	2	3	Cren	Cren'
Amazon River SPM																														
CBM5	78.4	4.5	1.6	12.6	1.6	0.2	0.7	0.2	–[a]	13.8	1.0	0.1	2.6	0.4	–	–	–	–	15.2	2.0	1.8	1.4	12.6	0.3	19.3	2.2	2.0	2.5	6.8	–
CBM6	22.1	2.2	0.8	4.1	0.7	–	0.4	–	–	1.6	0.3	0.1	0.5	–	–	0.1	–	–	7.9	3.5	4.5	4.1	38.7	1.2	5.0	0.9	1.7	2.7	4.7	–
CBM7	82.0	5.3	1.9	11.8	1.8	0.3	1.1	–	–	5.9	0.5	0.2	1.2	0.2	–	0.1	–	–	18.7	6.1	6.4	5.1	62.4	1.2	14.3	2.9	4.1	5.8	14.8	1.7
CBM8	49.6	5.1	1.7	10.7	2.2	0.4	1.0	–	–	11.5	0.6	0.2	1.2	0.2	–	0.1	–	–	11.0	2.8	3.3	2.9	28.6	0.8	8.1	1.4	2.0	2.8	6.7	1.1
Amazon River sediments																														
AMAZA 26	122.5	13.3	4.0	22.6	3.7	0.6	1.2	–	–	3.7	0.4	0.2	0.5	0.1	–	–	–	–	30.1	3.7	3.8	2.9	13.0	0.5	28.1	2.7	2.1	2.3	2.7	0.4
AMAZC RO11B	48.1	4.8	1.7	7.2	1.1	0.2	0.3	–	–	12.3	1.7	0.5	2.5	0.4	0.1	0.1	–	–	8.8	1.3	1.5	1.2	7.0	0.2	8.4	0.8	0.8	1.0	1.8	0.3
AMAZC RO3	72.2	7.9	2.4	13.8	2.4	0.3	0.8	–	–	2.8	0.4	0.1	0.7	0.1	0.0	0.1	–	–	23.6	3.0	3.5	3.2	10.1	0.4	23.3	1.7	1.4	1.6	1.9	0.3
Marine SPM																														
13a bottom	1.0	0.1	–	0.2	0.1	–	0.2	–	–	0.2	0.02	–	0.04	–	–	0.01	–	–	9.9	3.1	3.3	0.5	18.7	1.3	2.6	1.0	1.4	0.2	2.1	0.3
13a chl_{max}	–	–	–	–	–	–	–	–	–	0.1	–	–	–	–	–	–	–	–	1.3	0.9	2.4	0.9	10.4	0.8	1.2	0.7	1.5	0.8	6.0	0.6
20 bottom	1.0	0.03	0.02	0.1	–	–	0.01	–	–	1.1	0.1	0.03	0.2	–	–	0.1	–	–	4.7	1.8	1.9	0.2	8.9	0.7	2.1	0.5	0.3	–	0.9	0.3
20 chl_{max}	0.01	–	–	–	–	–	–	–	–	0.1	–	–	–	–	–	–	–	–	0.4	0.3	0.3	0.1	2.3	0.1	0.5	0.3	0.3	0.2	1.4	0.2
21 bottom	0.6	0.1	–	0.1	–	–	0.1	–	–	0.9	0.1	0.1	0.2	–	–	–	–	–	27.4	9.4	10.2	1.0	45.4	3.7	6.3	2.6	4.2	0.1	3.8	1.5
21 chl_{max}	0.2	0.02	–	0.04	–	–	–	–	–	0.1	–	–	–	–	–	–	–	–	3.9	2.2	2.4	1.1	20.2	1.2	4.7	3.3	3.7	2.2	28.1	2.3
22b bottom	0.04	–	–	–	–	–	0.1	–	–	0.1	–	–	–	–	–	–	–	–	3.1	1.1	1.2	0.1	5.3	0.4	2.0	1.0	1.7	0.05	1.6	–
22b chl_{max}	0.2	0.02	0.01	0.03	–	–	–	–	–	–	–	–	–	–	–	–	–	–	1.0	0.6	0.6	0.2	5.0	0.3	1.8	1.3	1.6	0.9	9.4	0.9
23 bottom	0.1	0.03	–	–	–	–	0.1	–	–	0.4	–	–	0.1	–	–	–	–	–	14.7	7.4	10.4	5.2	49.7	3.3	15.1	6.0	7.8	4.4	38.2	5.2
23 chl_{max}	0.02	–	–	–	–	–	–	–	–	0.02	–	–	–	–	–	–	–	–	0.3	0.3	0.5	0.3	2.7	0.1	0.2	0.1	0.2	0.1	1.0	0.1
25 bottom	18.6	3.5	1.6	3.8	0.8	0.2	0.3	–	–	0.02	–	–	–	–	–	–	–	–	7.5	2.8	3.8	2.2	33.1	1.2	5.8	1.5	2.1	1.6	12.0	1.6
25 chl_{max}	0.7	0.1	0.1	0.2	0.04	–	0.01	–	–	0.1	0.04	0.02	–	–	–	–	–	–	1.6	0.9	1.9	0.6	12.6	0.3	0.5	0.3	0.7	0.3	3.4	–
28b bottom	0.3	0.03	–	0.1	–	–	0.1	–	–	–	–	–	–	–	–	–	–	–	18.2	5.1	5.0	0.8	31.3	2.1	5.8	2.5	4.8	0.01	2.0	1.2
28b chl_{max}	0.04	–	–	–	–	–	–	–	–	0.1	–	–	–	–	–	–	–	–	4.5	2.4	4.8	2.0	22.7	2.2	8.0	4.4	5.9	2.8	37.1	2.5
32b bottom	0.2	–	–	0.1	–	–	0.3	–	–	0.4	–	–	–	–	–	–	–	–	12.3	4.7	4.6	0.5	22.3	1.7	6.0	3.4	5.9	0.3	5.0	–
32b chl_{max}	0.02	–	–	–	–	–	–	–	–	0.03	–	–	–	–	–	–	–	–	1.4	0.8	1.1	0.4	6.7	0.4	0.9	0.5	0.5	0.3	3.7	0.3
42b bottom	0.8	0.1	0.03	0.2	0.03	–	0.2	–	–	0.2	–	–	–	–	–	–	–	–	22.7	7.6	8.3	0.8	36.8	3.0	20.2	8.8	13.0	0.5	14.5	5.0
42b chl_{max}	0.1	–	–	–	–	–	–	–	–	0.1	–	–	–	–	–	–	–	–	1.7	0.8	1.2	0.3	7.2	0.5	1.4	0.8	1.0	0.5	5.8	0.5
42c/d bottom	0.1	–	–	0.03	–	0.04	0.2	–	–	0.1	–	–	–	–	–	–	–	–	10.0	3.7	5.4	0.8	23.4	2.4	7.3	2.8	6.2	0.6	9.4	5.1
42c/d chl_{max}	0.1	–	–	–	–	–	–	–	–	0.1	–	–	–	–	–	–	–	–	0.9	0.5	0.9	0.4	4.7	0.3	0.4	0.3	0.6	0.2	2.4	0.2
42d bottom	0.1	0.04	–	–	–	–	0.02	–	–	0.04	–	–	–	–	–	–	–	–	12.6	8.1	12.5	8.2	63.7	3.3	7.8	3.7	4.3	2.9	24.6	2.2
42d chl_{max}	–	–	–	–	–	–	–	–	–	0.03	–	–	–	–	–	–	–	–	0.3	0.2	0.4	0.2	2.1	0.1	0.2	0.1	0.2	0.1	0.8	0.1
43 bottom	0.2	0.2	0.1	0.2	0.1	0.04	0.1	–	–	0.1	0.04	0.03	–	–	–	–	–	–	2.1	1.7	3.2	2.4	24.2	0.7	0.7	0.5	0.7	0.5	3.9	–
43 chl_{max}	0.4	0.3	0.4	0.2	0.1	0.1	0.2	–	–	0.1	0.04	0.03	–	–	–	–	–	–	6.6	6.0	10.2	7.7	69.8	2.1	1.8	1.1	1.8	1.6	14.4	0.6
Marine surface sediments																														
13a	3.9	0.4	0.1	0.9	0.4	0.1	0.7	0.1	0.02	0.1	0.02	0.01	0.1	0.03	0.02	0.04	0.01	–	28.7	7.8	8.6	1.5	46.7	4.1	3.4	0.6	0.6	0.2	3.2	0.2
20	2.9	0.2	0.1	0.6	0.2	0.1	0.3	0.1	0.01	0.02	0.01	0.01	0.03	0.02	0.01	0.01	0.01	–	16.4	4.6	4.9	0.8	27.8	2.4	4.7	0.8	0.7	0.2	3.3	0.2
21	2.9	0.2	0.1	0.6	0.2	0.1	0.2	0.02	–	0.1	0.01	–	0.1	0.01	0.01	0.02	–	–	19.6	5.6	6.2	1.0	40.0	2.8	3.5	0.6	0.5	0.2	2.8	0.2
22b	6.0	0.5	0.2	1.3	0.5	0.1	0.4	0.1	–	0.3	0.1	0.02	0.2	0.1	0.03	0.03	–	–	35.1	10.4	11.4	2.0	53.3	5.0	7.9	1.3	1.1	0.3	6.6	0.4

23		3.7	0.3	0.1	1.0	0.2	0.1	1.6	0.1	–	0.3	0.1	0.02	0.1	0.03	–	0.1	0.01	–	43.9	10.9	11.0	1.5	74.6	4.8	8.5	0.8	0.8	0.2	4.9	0.4
25		46.5	9.1	4.3	10.8	2.0	0.4	0.6	0.1	–	1.6	0.3	0.1	0.3	0.1	0.02	0.02	–	–	13.2	4.3	6.2	3.8	56.2	2.4	6.8	1.4	2.2	1.6	15.0	1.4
28b		4.4	0.3	0.1	0.8	0.3	0.1	0.4	–	–	0.2	0.02	0.01	0.04	0.02	–	0.02	–	–	38.7	10.2	11.2	1.6	74.7	5.0	10.8	1.5	1.3	0.3	7.2	0.4
32c		2.3	0.2	0.1	0.5	0.2	0.1	0.5	0.03	0.01	0.1	0.01	0.01	0.1	0.02	–	0.02	–	–	25.7	7.3	8.2	1.2	48.3	3.8	4.3	0.5	0.5	0.1	2.8	0.2
32b		3.1	0.2	0.1	0.6	0.2	0.1	0.4	0.04	–	0.1	0.01	0.01	0.04	0.01	–	0.02	–	–	18.8	4.8	5.3	0.8	37.4	2.4	3.3	0.5	0.4	0.1	2.7	0.2
42b		17.6	1.1	0.4	3.0	0.8	0.2	0.6	0.1	–	0.4	0.1	0.02	0.2	0.1	0.03	0.02	–	–	17.4	4.3	4.6	1.0	35.1	2.2	7.7	1.2	0.8	0.3	5.6	0.3
42d		0.7	1.7	1.4	0.4	1.0	0.2	0.04	–	–	0.1	0.2	0.2	0.04	0.1	–	0.03	–	–	10.5	5.7	7.3	4.2	54.9	2.4	3.6	2.1	3.1	2.1	24.2	–
43		13.7	6.6	6.0	9.0	3.6	1.4	4.0	–	–	1.4	0.2	0.2	0.6	0.2	0.01	0.2	–	–	26.8	15.9	22.8	16.0	211.5	6.7	8.5	3.4	5.1	3.4	42.2	2.5
44c		3.5	0.3	0.1	1.0	0.2	0.1	1.7	0.1	–	0.1	0.02	–	0.1	0.02	0.01	0.1	–	–	37.4	10.0	10.1	1.4	71.3	4.8	6.5	0.7	0.8	0.2	4.6	0.4
49		0.6	0.1	0.02	0.2	0.1	0.02	0.4	0.03	–	0.03	0.01	–	0.01	0.01	–	0.01	–	–	14.6	3.7	3.7	0.5	24.3	1.5	3.9	0.4	0.3	0.1	2.1	0.1
54		61.4	1.9	0.5	8.2	0.9	0.2	1.7	0.2	0.1	0.2	0.03	0.01	0.2	0.1	0.03	0.2	–	–	12.0	2.1	1.9	0.3	15.7	0.8	3.4	0.3	0.2	0.1	1.5	0.1
60b		2.9	0.2	0.1	0.7	0.1	0.1	0.9	0.1	–	0.1	0.01	0.01	0.02	0.02	–	0.02	–	–	28.0	7.3	7.5	1.0	50.6	3.1	7.8	0.9	0.8	0.2	4.1	0.4

[a] "–" = below detection limit.
[b] isoGDGT 0–3 refere to GDGT-0 to GDGT-3 in Fig. 1.

the same range as the concentration in the river. However, the concentration per L was about 100 times higher in river SPM than in marine SPM (0.06 to 4 ng L^{-1} for the CL fraction and 0.03 to 1.7 ng L^{-1} for the IPL fraction). In the marine SPM, crenarchaeol was the most abundant isoGDGT (on average 56% of the total amount of all CL isoGDGTs). The GDGT-0/crenarchaeol ratio varied between 0.1 and 0.6 in the CL fraction. In the IPL fraction, the variation was larger, with values varying between 0.1 and 3.0 (Fig. 7A). The TEX_{86} varied from 0.59 to 0.83 in the CL isoGDGTs and from 0.65 to 0.81 in the IPL-derived isoGDGTs (Fig. 7B). The TEX_{86}-derived temperatures were 18–26 °C for CL isoGDGTs and 20–25 °C for IPL-derived isoGDGTs (Fig. 7C). The BIT values in marine SPM were in general low with values of 0–0.1 in the CL fraction. Only in the SPM of the bottom water of station 25 the BIT was higher (0.41). The BIT in the IPL fraction varied between 0 and 0.53 (Fig. 7D).

4.3. Marine sediments

In the marine surface sediments the brGDGT concentrations varied between 2 and 74 μg g_{OC}^{-1} in the CL fraction and between 0.1 and 2.7 μg g_{OC}^{-1} in the IPL fraction (Fig. 3A and B, Table 2). IPL-derived brGDGTs represented on average 5% of the total brGDGTs. The highest concentrations were found at stations 25 and 43, the two sampling stations closest to the Amazon River mouth (Fig. 2D). Surprisingly, high concentrations were also found at station 54. The distribution of brGDGTs varied widely (Fig. 4C); in general GDGT Ia was most abundant, but its relative abundance varied from 11% to 80% in the CL brGDGTs and from 16% to 36% in the IPL-derived brGDGTs (Table 2). The second most abundant brGDGTs was either IIa or IIIa. The MBT of the core-top sediments varied between 0.48 and 0.85 (CL brGDGTs) and between 0.35 and 0.81 (IPL-derived brGDGTs) (Fig. 5A). The DC was between 0.04 and 0.72 (CL brGDGTs) and between 0.13 and 0.55 (IPL-derived brGDGTs) (Fig. 5B). The highest values were found at the stations 42d and 43, where higher pH values (~9) were also measured than at other stations (~8) (Table 1). The CBT-derived pH varied from 4.9 to 8.0 in the CL brGDGTs and from 6.0 to 7.5 in the IPL-derived brGDGTs (Fig. 5C). The MBT/CBT-derived MAAT ranged from 12 to 23 °C in the CL brGDGTs and from 6 to 23 °C in the IPL-derived brGDGTs (Fig. 5D).

IsoGDGT concentrations in the marine surface sediments varied between 32 and 300 μg g_{OC}^{-1} for the CL fraction and between 5 and 65 μg g_{OC}^{-1} for the IPL fraction (Fig. 3C and D, Table 2). IPL-derived isoGDGTs represented 14% of the total isoGDGTs. In marine sediments, the most common isoGDGT was also crenarchaeol (e.g. Fig. 6B) in both the CL fraction (52%) and the IPL fraction (39%). The ratio between crenarchaeol and GDGT-0 varied between 0.13 and 0.76 in the CL GDGTs and between 0.15 and 2.20 in the IPL derived GDGTs (Fig. 7A). The TEX_{86} varied between 0.6 and 0.74 in the CL isoGDGTs and between 0.5 and 0.79 in the IPL-derived isoGDGTs (Fig. 7B). The TEX_{86}-derived temperatures were 19–24 °C for CL isoGDGTs and 14–25 °C for IPL-derived

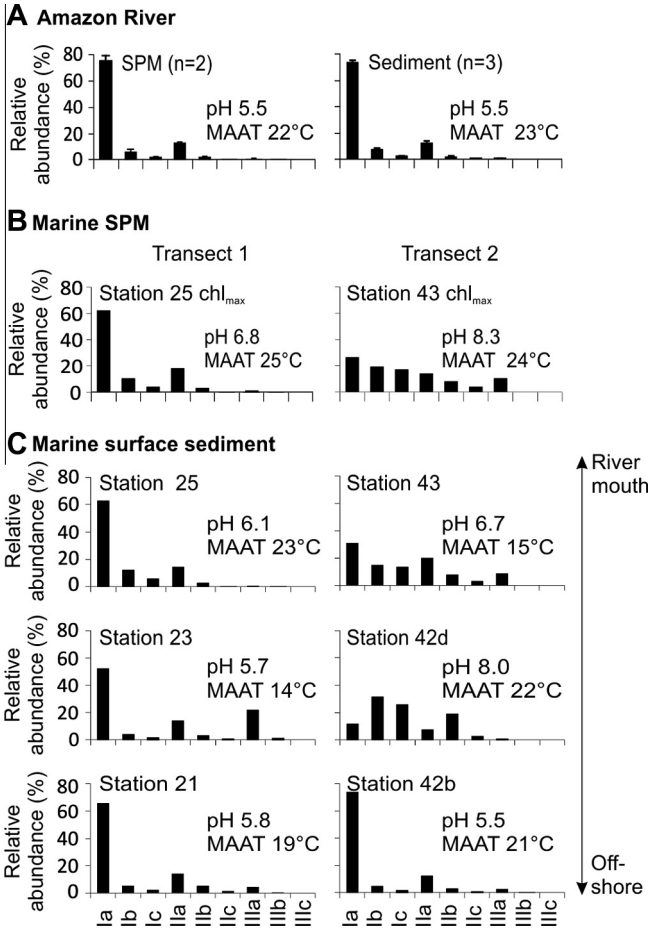

Fig. 4. Average CL brGDGT distribution in (A) Amazon River SPM and sediments and in (B) marine SPM and (C) surface sediments from 3 stations closest to the shore from the two studied transects (Fig. 2D). Also indicated are the respective CBT-derived pH and MBT/CBT-derived MAAT values. Vertical bars indicate the standard deviation (1δ).

isoGDGTs (Fig. 7C). Surprisingly, the highest BIT value of the CL GDGTs was found at station 54 with a BIT of 0.78 (0.20 for IPL-derived GDGTs) and not at station 25, which had a BIT of 0.37 (0.11 of IPL-derived isoGDGTs). At all other stations the BIT was lower, varying between 0.06 and 0.12 for CL GDGTs and between 0.01 and 0.07 for IPL-derived GDGTs (Fig. 7D).

4.4. IPL GDGTs

Chl_{max} and bottom water SPM and marine sediments from four stations (25, 28b, 42d, and 43) were analyzed for intact IPLs. BrGDGTs with polar head-groups were only detected at stations 25 and 42d. The detected brGDGT IPLs were glyconyl-brGDGT I (1, numerals refer to Fig. 1), phosphohexose-brGDGT I (2), and hexose-phosphoglycerol-brGDGT I (3). All three brGDGT IPLs were found in the sediment of station 25. In the bottom SPM IPLs 2 and 3 were found, while at the chl_{max} compound 1 was detected. At station 42d the sediment contained compound 2 and 3, while the SPM contained compound 1. Crenarchaeol IPLs were detected in SPM and sediments of all four tested stations. The following crenarchaeol-derived IPLs were detected: crenarchaeol-monohexose (4), crenarchaeol-dihexose (5), and crenarchaeol-hexose-phosphohexose (6). The relative amount of the respective IPLs is reported in Table 3.

5. DISCUSSION

5.1. Origin of brGDGTs on the Amazon shelf and in the Amazon fan

It has been assumed that the brGDGTs in marine sediments are mainly derived from erosion of soils and are transported through rivers to the coastal marine environment (Weijers et al., 2007a). Hence, it is expected that the highest concentrations of brGDGTs normalized to OC are to be found in the river and close to the river mouth and then should decrease gradually offshore until brGDGTs can no longer be detected (cf. Hopmans et al., 2004). It is also anticipated that the distribution of the nine brGDGTs derived from soil is preserved in coastal marine sediments, without a substantial alteration of the brGDGT distribution (Weijers et al., 2007a). Zell et al. (2013a) examined the distribution of brGDGTs in 'terra firme' soils from

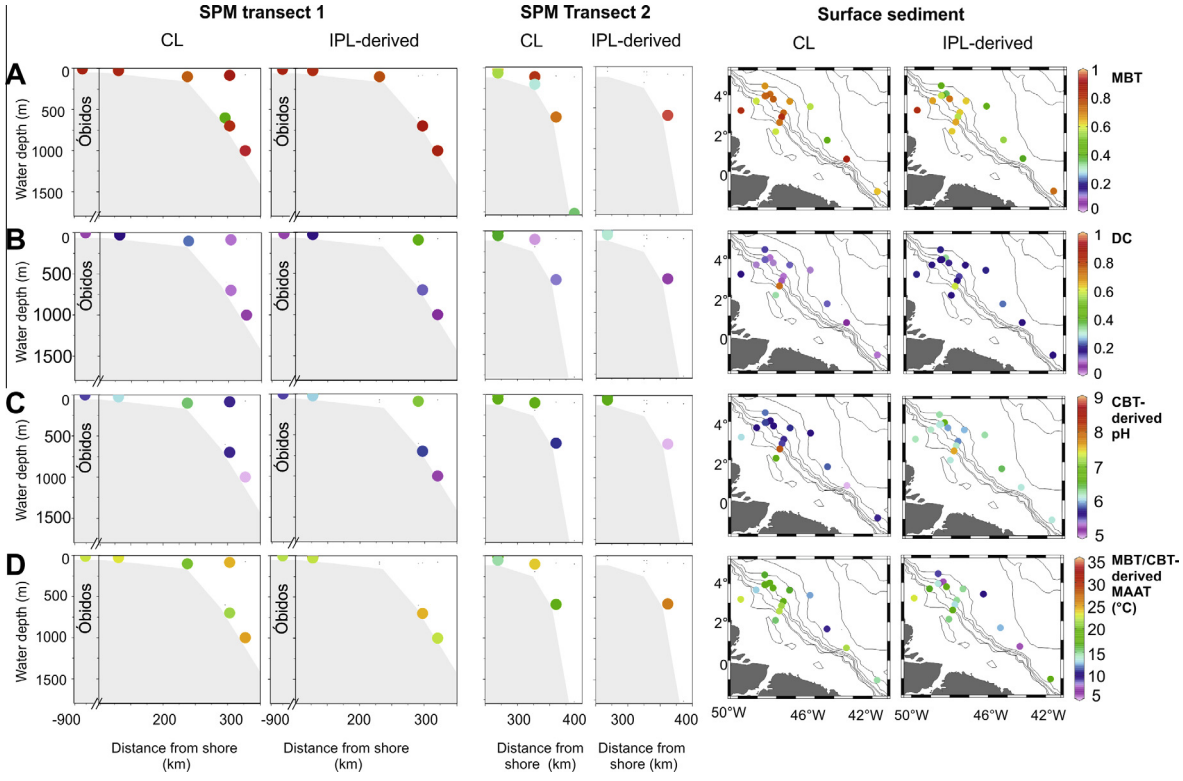

Fig. 5. MBT (A), DC (B), and CBT-derived pH (C), and MBT/CBT-derived MAAT values (D) in riverine and marine SPM (transects 1 and 2; Fig. 2D) and in marine surface sediments.

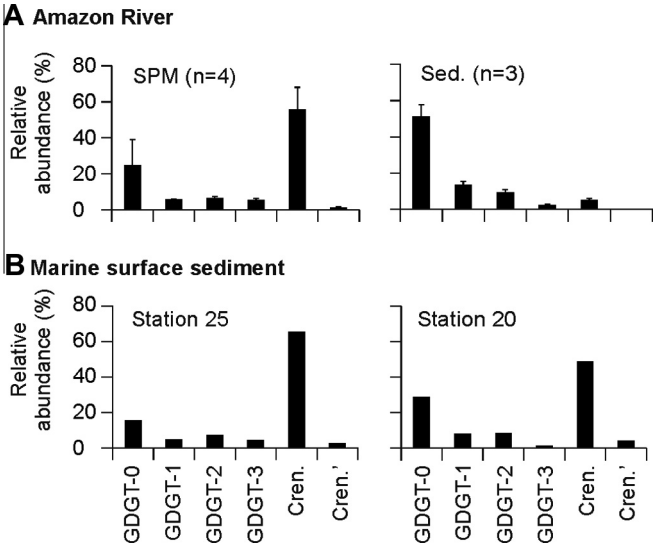

Fig. 6. Average CL isoGDGT distribution in (A) Amazon River SPM and sediment, and in two marine surface sediment (B). Vertical bars indicate the standard deviation (1δ).

the Amazon watershed and compared it against brGDGTs in river SPM. They found that the brGDGT distribution in river SPM was slightly different from that in the lowland soils, most likely due to additional in situ production of brGDGTs within the Amazon River. In the present study, we concentrate on examining the second step: the delivery of brGDGTs to the ocean by the Amazon River.

The concentrations of the CL brGDGTs normalized to OC in Amazon River SPM and Amazon sediment (Table 2) and the distributions of CL brGDGTs in river SPM and sediments were similar (Fig. 4A). That the distributions were similar is also apparent from the fact that these samples plot close vicinity to each other in a brGDGT "provenance plot" (i.e. a plot of DC vs. MBT, Fig. 8A; cf.

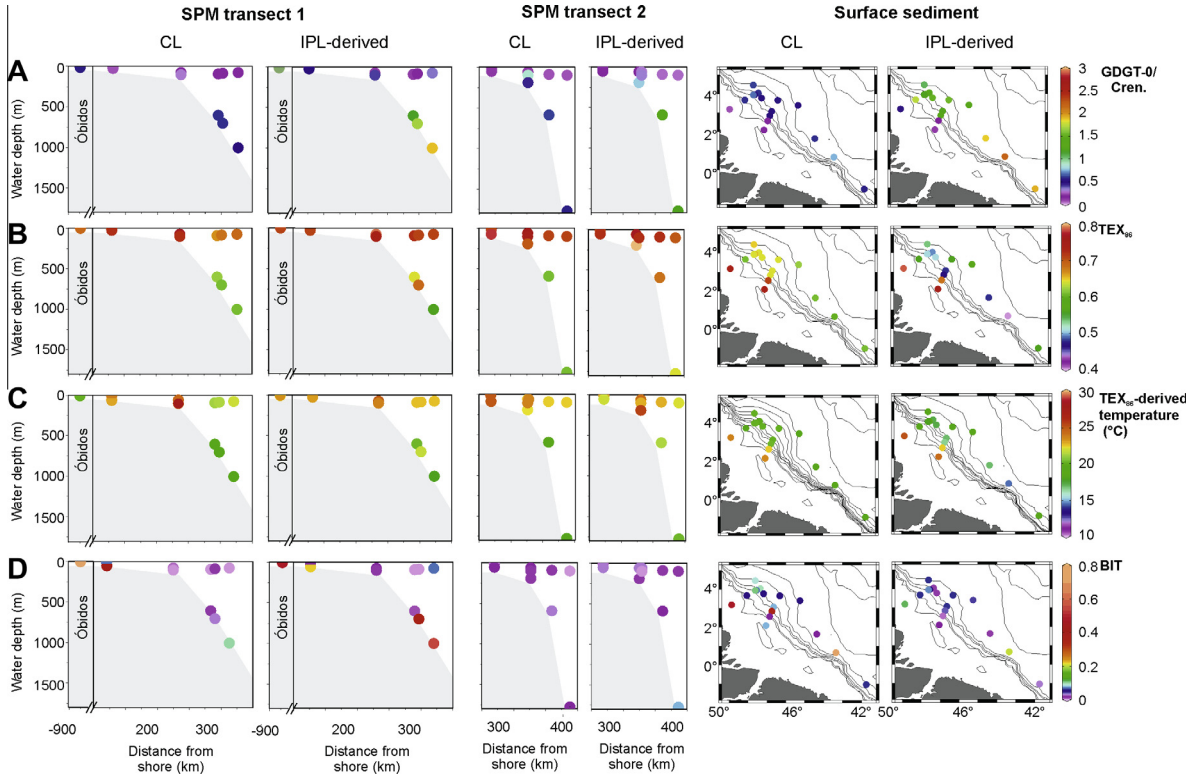

Fig. 7. GDGT-0/crenarchaeol ratio (A), TEX_{86} values (B), TEX_{86}-derived temperature (C), and BIT index values (D) in riverine and marine SPM (transects 1 and 2; Fig. 2D) and in marine surface sediments.

Sinninghe Damsté et al., 2009). The distribution (Fig. 8A) and the average percentage of IPL-derived brGDGTs (11% and 7%, respectively) were also similar in the Amazon River SPM and sediment. Since the SPM and one riverbed sediment were collected close to the town of Óbidos and the two other riverbed sediments were collected farther downstream (Fig. 2A), our results also show that there is no alteration of the brGDGTs between Óbidos and shortly before the river mouth.

On the Amazon shelf, station 25 is the station that was mostly strongly influences by the Amazon River water, because of the NW deflection of the river plume caused by the North Brazilian Current (Fig. 2D). The CL brGDGT concentration in the surface waters at station 25 was lower than in the deeper waters (Fig. 3A, Table 2), but at both depths in station 25 the CL brGDGT distribution was similar to that of Amazon River SPM (Fig. 8A). The marine SPM at the other sites had 50 to 1000 times lower CL brGDGT concentrations (normalized to OC) and most of them had a different CL brGDGT distribution than the river SPM (Fig. 8A). The MBT of most marine SPM was lower than that in the Amazon River (Fig. 8A). The DC of marine SPM was variable but relatively high (>~0.3) at stations 28b, 42d, and 43 (Fig. 8A) compared to the other stations. Station 43 is the station of transect 2 which is closest to the shore (Fig. 2D), but clearly showed a much higher DC in both chl_{max} and bottom water SPM compared to the DC of CL brGDGTs in the Amazon River (Figs. 4 and 5A and B, 8A). Only four SPM samples contained sufficient IPL-derived brGDGTs (stations 13, 20, 21, and 25) to determine the MBT and DC. In contrast to CL brGDGTs, they showed MBT and DC values similar to those found in the Amazon River (Fig. 8A).

Similar observations were made for the marine surface sediment; the sediments from the two stations closest to the river mouth (stations 25 and 43; Fig. 2D) had high CL brGDGT concentrations normalized to OC compared to those of the other stations (Fig. 3A). Of these two stations only the brGDGT distribution at station 25 was similar to that of the Amazon River (Fig. 8A). Station 54 also had a surprisingly high CL brGDGT concentration (Fig. 3A) and a MBT and DC similar to that of the Amazon River (Fig. 8A), even though it is unlikely that it is influenced by the Amazon River since the ocean current flows northwards (Fig. 2). We assume that this station receives brGDGTs from the Bacanga River, a river southeast of the Amazon basin, which enters the ocean at the city of São Luis (S 2.5°, W 44.3°) and probably delivers brGDGTs to the ocean with a distribution that is comparable to that found in SPM of the Amazon River. In the other marine sediments the CL brGDGT concentration was lower (Fig. 3A) and the distribution of CL brGDGTs varied strongly (Fig. 4C), resulting in substantial differences in MBT and DC values (Figs. 5A and 8A). The sediment of the shelf stations 43 and 42d were special as they exhibited exceptionally high DC values (Fig. 8A). Almost all sediments had a lower MBT compared to the Amazon River. The MBT showed a tendency to decrease with increasing

Table 3
Percentage of the total detected IPLs with a brGDGT (Ia) and crenarchaeol core, assuming similar response factors for the different IPLs, in SPM and marine surface sediment at selected stations.

Station	25			28b			42d			43		
IPLs[a]	Chl_{max} SPM	Bottom SPM	Sediment	Chl_{max} SPM	Bottom SPM	Sediment	Chl_{max} SPM	Bottom SPM	Sediment	Chl_{max} SPM	Bottom SPM	Sediment
Ia												
1	100	0	10	–	–	–	100	100	0	–	–	–
2	0	91	76	–	–	–	0	0	66	–	–	–
3	0	8.7	14	–	–	–	0	0	34	–	–	–
Crenarchaeol												
4	31	33	29	34	10	19	10	55	52	37	25	32
5	3	32	10	6	85	5	2	19	39	6	3	48
6	66	35	61	60	5	76	87	26	9	57	73	21

"–" = below detection limit.
[a] Numbers refer to structures shown in Fig. 1.

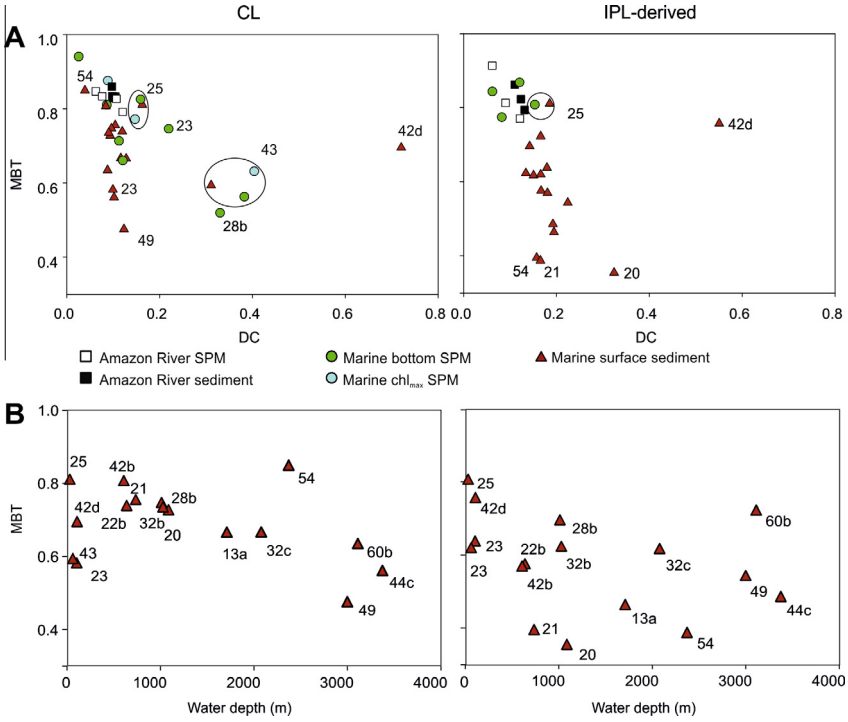

Fig. 8. MBT vs. DC cross plot (A) to compare the distributions of CL and IPL-derived brGDGTs of all analyzed riverine and marine SPM and sediment samples and (B) the relationship of MBT with water depth in marine surface sediments.

water depth (Fig. 8B). Changes in DC and MBT were also evident in the IPL-derived brGDGTs. Their DC values were generally slightly higher than those of the CL brGDGTs (Fig. 8A). However, only one of the two stations (i.e. 42d) which were characterized by substantially higher DC values in the CL brGDGTs also showed a higher DC in the IPL-derived GDGTs (Fig. 8A). MBT values of IPL-derived brGDGTs were generally lower and more variable. No decrease with water depth was apparent (Fig. 8B). A ternary plot showing the relative abundance of the various groups of brGDGTs (Fig. 9A) reveals that in most SPM and surface sediments lower MBT values for CL brGDGTs are due to higher relative amounts of II(a–c) and III(a–c). The same can be seen in the IPL-derived brGDGTs (Fig. 9B), but in the IPL-derived brGDGTs the fraction of brGDGT II(a–c) varies to a larger extent than the CL brGDGT III(a–c).

Our results show that there are major changes in the brGDGT distribution from the Amazon River to marine SPM and sediment and also within the marine environment. This is most likely caused by selective degradation processes of brGDGTs derived from the terrestrial environment or by in situ production of brGDGTs in the marine environment, or both. Furthermore, seasonal variations in hydrodynamics in the river catchments (Zell et al., 2013b) or, perhaps, input by eolian transport (Fietz et al., 2013)

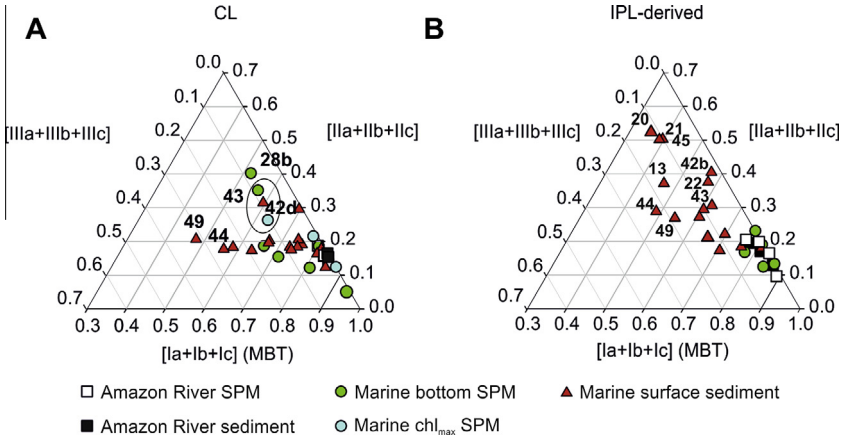

Fig. 9. Ternary plot showing the relative amount of the sum of brGDGT I(a–c), II(a–c), and III(a–c) in all analyzed samples for (A) CLs and (B) IPLs.

might play a role in altering the riverine brGDGT signals in marine settings. Intensive degradation of organic compounds take place on the Amazon shelf where it was previously shown that 55–70% of the POC flux from the Amazon River is decomposed or otherwise lost before being buried in sediments (Aller et al., 1996). Long residence times of organic-rich particulates in deltaic "fluid muds" underlying oxygenated water makes the Amazon shelf region relatively inefficient for organic carbon preservation (Blair and Aller, 2012). Oxic degradation might presumably affect the brGDGTs, but the brGDGT delivered from the river should have been affected in a similar way. Therefore, it seems unlikely that the large differences of the brGDGT distributions between marine surface sediments and SPM can be explained solely by microbial degradation. Hydrodynamic processes in the Amazon Basin slightly altered brGDGT distributions of the Amazon River SPM (Zell et al., 2013b). However, the riverine brGDGT data obtained at the Óbidos station, the last gauging station in the Amazon River, very closely clustered together, separated from those of the most of the marine SPM and sediments. Therefore, it is unlikely that hydrodynamic processes occurred in the Amazon basin are solely responsible for variable distributions of brGDGTs observed in the Amazon shelf and fan. Recently, Fietz et al. (2013) showed that atmospheric dust samples collected off northwest Africa contained brGDGTs and thus an eolian input of brGDGTs might also influence brGDGT signals, especially in remote open ocean settings. However, the eolian input of brGDGTs is also unlikely due to the heterogeneous distribution of brGDGTs observed in coastal marine SPM and sediments in our study area.

In-situ production of brGDGTs in the marine environment is an alternative explanation. Marine in situ production of brGDGTs has previously been proposed in coastal sediments of Svalbard (Peterse et al., 2009), in East China Sea shelf sediments (Zhu et al., 2011), and in hydrothermal vents in the south Pacific Ocean (Hu et al., 2012). A higher amount of cyclic brGDGTs, similar to what we observed in SPM and sediment of the Amazon shelf, was observed in the coastal sediments of Svalbard and East China Sea shelf sediments. However, Zhu et al. (2011) reported that the MBT increased from the Yangtze River sediment to coastal sediment, which is opposite the trend we observe for the Amazon system.

In order to investigate whether marine in situ production causes the difference between the brGDGT distributions in the Amazon River, compared to that in the marine environment, we analyzed IPL-derived brGDGTs. IPL-derived brGDGTs are more labile compared to CL brGDGTs, since the polar head group of IPL brGDGTs is lost relatively fast (within days) after cell death (Harvey et al., 1986; Logemann et al., 2011). Therefore, IPL-derived GDGTs are considered to represent the more recently produced, 'fresher' brGDGTs than CL brGDGTs. The percentage of IPL-derived brGDGTs of the total amount of brGDGTs might indicate where increased production of brGDGTs occurs. In marine SPM, the percentage of IPL-derived brGDGTs was substantially higher (43%) than that in the river (7%) and in marine sediments (5%). This higher percentage in marine SPM might indicate that brGDGTs are at least partially produced in the water column and potentially sink down to the sediments where they are preserved as CLs. However, the MBT and DC values of IPL-derived brGDGTs in marine SPM were similar to those found in the IPL-derived brGDGTs in the Amazon River (Fig. 8A), which would suggest that the brGDGTs produced in the marine water column are similar to the brGDGTs in the river and that the different distribution of the CL brGDGTs must derive from another source. However, these results should be interpreted with care, since there were only four SPM samples that contained sufficient amounts of IPL-derived brGDGTs to calculate the MBT and DC. Of the marine sediments, station 42d sediment had the highest percentage of IPL-derived brGDGTs, this was also the only station besides station 25 in which IPLs could be directly detected. The detected IPLs included phospholipids which are known to degrade faster than glycolipids (Harvey et al., 1986; Lengger et al., 2012), which suggests that at least some of the IPL-derived GDGTs were recently produced. The DC of IPL-derived brGDGTs in marine sediments was slightly higher than that of the

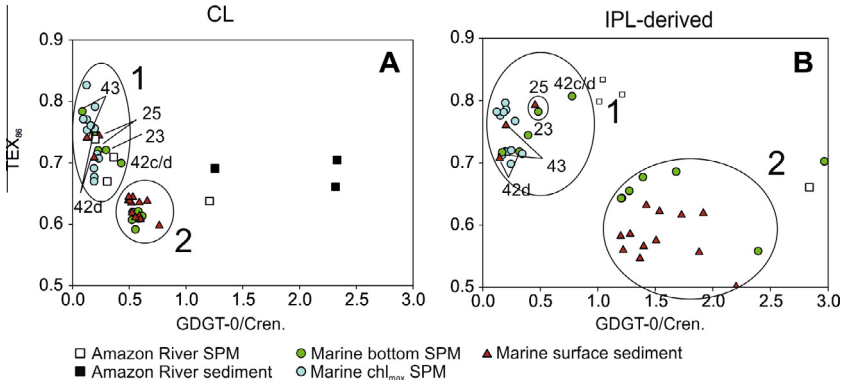

Fig. 10. GDGT-0/crenarchaol ratio vs. TEX_{86} cross plot showing the differences in isoGDGT distribution of the different sample types: (A) CL isoGDGTs and (B) IPL-derived isoGDGTs. The data of the Amazon River sediments are not shown in (B) because the GDGT-0/crenarchaeol values were much higher than those of the other samples (GDGT-0/crenarchaeol ratio = 4, 10, and 12, TEX_{86} = 0.70, 0.64, and 0.67, respectively). Clusters 1 and 2 are discussed in the text.

Amazon River, except for the sediment of station 42d in which it was much higher (Fig. 8A). The higher DC was associated with higher sediment pH at stations 42d and 43 (Table 1). This might indicate that the DC of brGDGTs produced in the marine environment, like the DC of soil brGDGTs (Weijers et al., 2007b), is related to the environmental pH. If we assume that this is the case, the brGDGT distributions at stations 42d and 43 would be a strong indication for marine in situ production at these sites. The CBT-derived pH from station 42d was not as high as the measured pH, but this could be due to a flattening of the CBT–pH relationship at higher pH values as proposed by Xie et al. (2012). In addition, it is probable that the calibrations made for soils are not valid for the marine environment. In previous studies, it has been found that an increase of cyclic brGDGTs may be related with marine in situ production (Peterse et al., 2009; Zhu et al., 2011) which might be associated with the fact that the pH in the marine environment is typically higher than that of soil.

The MBT of IPL-derived brGDGTs in most marine surface sediments showed reduced values (0.4–0.75) compared to the river signature (0.8–0.9; Fig. 8A). In contrast to the CL brGDGTs an apparent decrease of the MBT with water depth cannot be observed in the IPL-derived brGDGTs (Fig. 8B). However, in the IPL fraction higher relative amounts of GDGT II(a–c) are evident from the ternary plot (Fig. 9B) compared to the CL brGDGTs in marine surface sediments from deep water. This might indicate that the processes that alter the brGDGT distribution in marine settings are more complex and might not only be influenced by in situ production. Another factor could be that the brGDGT distribution in the IPL-derived brGDGTs is not the same as that of the CL brGDGTs. For example, Lengger et al. (2012) showed that the TEX_{86} values of different isoGDGT IPLs is different. As some isoGDGT IPLs degrade faster than others, the TEX_{86} of the IPL fraction was consistently higher than that calculated with CL isoGDGTs. We assume that this could also be the case for brGDGTs, leading to a different MBT and DC in IPL-derived brGDGTs, compared to CL brGDGTs.

Overall our results show that brGDGTs are transported from the Amazon River to the ocean. However, only the brGDGT distribution of marine SPM and surface sediments in stations closest to the river source is similar to that in the river. Further away from the river, the brGDGT distribution in marine sediments varies widely. The major reason for this seems to be marine in situ production of brGDGTs with a variable distribution, which seems to be influenced by the pH and potentially lower temperatures in deeper water. This illustrates that the distribution of brGDGTs produced in the ocean may also correspond to the ambient environment.

5.2. Origins of isoGDGTs on the Amazon shelf and in the Amazon fan

Unlike the case of the brGDGTs, the concentration of CL isoGDGTs per g OC in the Amazon River SPM is similar to that in the ocean (Fig. 3C), but the concentration per liter was about 10–100 times higher in the river (Amazon River SPM on average: 60 μg L^{-1}, marine SPM at station 25: 3 μg L^{-1} and marine SPM at all other stations: 0.5 μg L^{-1}). Similar values have been reported for other river systems, e.g. the Rhine River (Herfort et al., 2006). This indicates that the Amazon River may act as a source of isoGDGTs in the marine environment. To determine if the riverine isoGDGTs influence the isoGDGT distribution in marine SPM and sediments, the GDGT-0/crenarchaeol ratio and the TEX_{86} values were compared (Fig. 10). The main difference between Amazon SPM and river-bed sediments was found in the relative amount of GDGT-0 and crenarchaeol. Crenarchaeol is only produced by Thaumarchaeota, while GDGT-0 is produced by many archaea, including Thaumarchaeota. Methanogenic archaea produce predominantly GDGT-0 (e.g. Schouten et al., 2013a,b). In Thaumarchaeota, the GDGT-0/crenarchaeol ratio is temperature-dependent, and typically varies between 0.2 and 2 (Schouten et al., 2002). It has been proposed for lakes, that if this ratio is >2 it indicates a substantial methanogenic origin of GDGT-0 (Blaga et al., 2009).

The values of the CL GDGT-0/crenarchaeol ratio were low (<1.5) in the river SPM, but in two out of three Amazon River sediments the values were slightly >2 (Fig. 10A). In the IPL-derived isoGDGTs from the three river-bed sediments, the GDGT-0/crenarchaeol ratio was even much higher (GDGT-0/crenarchaeol ratio = 5–13, the data are not shown in Fig. 10B). It is thus likely that methanogens from anoxic sediments in the Amazon system (Conrad et al., 2010) contribute to the GDGT signal in river sediments. However, these isoGDGTs in river sediments are only to a minor extent contributing to the isoGDGTs transported by the river since GDGT-0/crenarchaeol ratios of SPM for both the IPL and CL fractions are much smaller (Fig. 10).

When the GDGT-0/crenarchaeol ratio and TEX_{86} of the river SPM were compared to those of the marine SPM and sediments (Fig. 10A), it is observed that the GDGT-0/crenarchaeol ratio was higher in the river. TEX_{86} values of river SPM and sediment fell between those of marine SPM and sediments, which showed a wider range. CL values of isoGDGTs from the marine samples occurred in two clusters (Fig. 10A). The first cluster contained chl_{max} SPM of all stations, as well as bottom SPM and surface sediments of stations 25, 43 and 42d. The second cluster was formed by offshore bottom SPM samples and sediments. IPL-derived isoGDGTs showed more variation in TEX_{86} values but a similar clustering (Fig. 10B). The different IPL-derived isoGDGT distributions in offshore chl_{max} SPM compared to offshore bottom SPM and sediment suggests production of isoGDGTs below the chl_{max}. The higher GDGT-0/crenarchaeol ratio and the lower TEX_{86} values in cluster 2 may be explained by an increased contribution of Thaumarchaeota residing in deeper water. The more distinct appearance of this second cluster in IPL-derived isoGDGTs (Fig. 10B), supports the idea that isoGDGDTs are indeed produced in situ below the chl_{max}. This hypothesis is supported by the detection of crenarchaeol-hexose-phosphohexose, which is less stable than the other two crenarchaeol IPLs (Lengger et al., 2012), in these samples.

5.3. Implications for the use of GDGT-based paleoproxies in marine sediments

5.3.1. BIT

The flux-weighted value of the BIT index of SPM at Óbidos is 0.67 (Zell et al., 2013b) and the average BIT value of the river-bed sediments is 0.74. This is lower than the BIT index of lowland Amazon soils (0.9 on average), which is attributed to production of crenarchaeol in the Amazon River (Zell et al., 2013a,b). In the marine environment, the highest value of the BIT index was found in surface sediments at station 25 (0.50), at station 42b (0.36) and, surprisingly, also at station 54 (0.78), which is distant from the Amazon River. It is possible that the high concentration of brGDGTs measured at station 54 is due to the influence of the Bacanga River, which has its outflow further to the south. In agreement with this is that the brGDGT distribution observed at this station is similar to that of river SPM (see Section 5.1). In all other marine SPM samples and surface sediments, the BIT index was much lower, likely due to the substantially lower brGDGT concentrations (normalized on OC; Fig. 3A, Table 2). It has been reported for various systems that variations in the BIT index in marine SPM and sediments predominantly reflect variations in marine production of crenarchaeol rather than in the delivery of riverine brGDGTs (e.g., Weijers et al., 2009b; Fietz et al., 2011; Smith et al., 2012). However, in the Amazon River fan we generally observe relatively constant crenarchaeol concentrations (Fig. 3C, Table 2) in combination with sharply declining (with increasing distance from the river mouth) brGDGT concentrations, arguing for a dominant control of the delivery of brGDGTs from the river on the BIT index values. Despite the advocated potential in situ production of brGDGTs, it is still possible to use the BIT to detect riverine input apparently because the amounts of brGDGTs produced in situ in the marine environment are substantially lower than that of crenarchaeol.

5.3.2. The MBT/CBT paleothermometer

In order to be able to use the MBT/CBT as a continental temperature proxy, it is essential that the brGDGT distribution from soils is not altered during the transport and deposition of marine sediments. However, it has been shown that there is already a difference in the distribution of brGDGTs between Amazon basin soils and Amazon River SPM, due to in situ production in the river itself (Zell et al., 2013a,b). In the present study we found even more variable brGDGT distributions in marine SPM and surface sediments of the Amazon shelf and fan. Consequently, the MBT/CBT-derived pH and MAAT from the brGDGTs in most of the marine surface sediments using the Amazon soil calibration did not represent those of the Amazon drainage basin. In the marine environment, the highest CBT-derived pH (8) was 2.5 pH units higher than that of the Amazon River SPM (pH 5.5), whereas the MBT/CBT-derived MAAT was up to 14 °C colder than that of the Amazon River SPM. However, station 25, which was characterized by the highest OC-normalized brGDGT concentration (and high BIT index; 0.5) provided MBT/CBT-reconstructed MAAT and pH values comparable to the results obtained from the Amazon River watershed (Fig. 5D). Hence, it can be concluded that although most of the stations were only weakly influenced by the Amazon River outflow, the stations under high river influence still possess the "continental" Amazon brGDGT distribution. This suggests that the MBT/CBT proxy should only be used to reconstruct paleoenvironmental conditions from sediment cores that are demonstrably strongly influenced by the fluvial inputs of brGDGTs. In general, the BIT index may serve as a good, initial indicator for screening potential sites which are under strong fluvial influences.

Our new data allow us to re-evaluate the results obtained from ODP Site 942 (Bendle et al., 2010), a site that was used to reconstruct the climate of the Amazon basin during the late Quaternary. ODP Site 942 (Fig. 2, 5°45′N, 49°6′W, 3346 m water depth) is situated slightly north of the stations of the present study. The MBT/CBT-derived temperature (ca. 17 °C) of the surface sediments from their

study compares well with the temperatures derived from our surface sediments that were located closest to ODP Site 942 (our sites 13a, 20, and 21; Fig. 2D). Their MBT/CBT-derived temperature record showed relatively constant values of around 21 °C between 40 and 10.5 ka with a temperature drop just after 10.5 ka to values as low as 10 °C. This was followed by a general increase to 17 °C in the last 6 ka. The unexpected temperature drop of the early Holocene was explained by an increased input of brGDGTs from Andean soils, which would carry a "low temperature" signal (Bendle et al., 2010). This seems to be a conceivable argument, since ~82 to 95% of the suspended sediments in the Amazon River is currently derived from the Andes (e.g. Meade, 1994; Wittmann et al., 2011). However, the MBT/CBT-derived temperature from modern Amazon River SPM were higher (22 °C) than the temperatures derived from marine surface sediments and the brGDGT distribution from the river did not resemble the brGDGT distribution in the high Andes (Kim et al., 2012b; Zell et al., 2013a). Therefore, a major influence of brGDGTs from the Andean soils can be excluded, both today and presumably during the past. With our detailed data set on surface sediments in this area, we surmise that sea level changes had a significant impact on the MBT/CBT-derived temperature record of ODP Site 942. During a much reduced sea level stand, between 40 and 10.5 ka, river SPM could reach OPD Site 942 more directly than during the sea level high stand of the Holocene when the input of riverine SPM to ODP Site 942 was nil. This undoubtedly led to a much stronger influence of in situ produced brGDGTs on the MBT/CBT temperature record during the Holocene. This interpretation is supported by the BIT record which showed high values (ca. 0.6) from 40 to 10.5 ka and a subsequent reduction in the Early Holocene. However, the BIT values during the Holocene for this core remain remarkably high (ca. 0.3), indicating that the BIT index should be used with caution as an indicator for the applicability of the terrestrial MBT/CBT palaeothermometer. In conclusion, in order to reconstruct the MAAT of the Amazon basin during the Holocene, a core site near to the Amazon River mouth, where more riverine terrestrial material is being deposited should be considered.

The comparison of our results with those of similar studies showed that there might be substantial differences between river systems. So far, two other river systems have been studied for the applicability of the MBT/CBT as a paleothermometer in marine sediments, i.e. the Yangtze River and the Pearl River in China (Zhu et al., 2011; Strong et al., 2012; Zhang et al., 2012). In the marine sediments of these river systems, like in the Amazon River system, MBT/CBT-derived MAATs were lower than the actual MAATs of the drainage basins. In addition the cause of lower MBT/CBT-derived MAATs was different in the two Chinese rivers. In front of the Yangtze River, DC values increased, but lower MBT values were not found (Zhu et al., 2011). In the Pearl River, DC and MBT changes between the soil, river and marine sites were not obvious (Strong et al., 2012; Zhang et al., 2012). This suggests that the applicability of the MBT/CBT proxy can vary between different river systems, potentially due to the differences in the sedimentary regimes, hydrodynamics, and degradation loss (Strong et al., 2012), but also differences between the populations of brGDGT producing bacteria. We conclude that it is necessary to investigate recent samples from a river system before applying the MBT/CBT proxy and we suggest caution in the application of the proxy to past periods of low sea level and changing delivery rates of riverine sediments to marine depositional sites.

5.3.3. The TEX_{86} paleothermometer

Since the TEX_{86} values for Amazon River SPM and for marine SPM at the chl_{max} and surface sediments were similar, the influence of riverine isoGDGTs on the TEX_{86} could not be detected in our study area. All marine samples (except for station 25) had a BIT value <0.2 and a GDGT-0/crenarchaeol ratio <2. This means that their TEX_{86} values should record the sea temperature of the top 200 m water column (Weijers et al., 2006b; Kim et al., 2012a). TEX_{86}-derived temperatures from the chl_{max} SPM were about 24 °C (average water depth chl_{max} = 72 m) compared with the depth-integrated temperature between 0 and 100 m of 27 °C (WOA09 data base). Therefore, the TEX_{86}-derived temperatures were ca. 3 °C lower than expected; we should note that the temperature reconstructed from the SPM is a snap shot and not the annual mean. However, since the sampling site is close to the equator, no strong seasonal temperature changes are expected. In offshore bottom SPM and sediments, TEX_{86}-derived temperatures were even lower (20 °C), possibly due to the influence of isoGDGTs produced below the chl_{max}. This led to TEX_{86}-derived temperatures that were on average 4 °C colder than the depth-integrated annual mean temperatures from 0 to 200 m water depth (Table 1). The detection of crenarchaeol-hexose-phosphohexose in marine SPM and sediments also indicates that the in situ production of isoGDGTs in sediments might occur in the Amazon shelf and fan. However, the sedimentary production of isoGDGTs is unlikely to influence the TEX_{86}, because the majority of isoGDGTs is derived from the water column and the isoGDGTs produced in sediments might be more easily degradable (Lengger et al., 2012).

6. CONCLUSIONS

Our study shows that brGDGTs are primarily transported from the Amazon River to marine sediments. However, brGDGTs are also produced in the marine environment. Hence caution has to be taken when using the MBT/CBT proxy in marine sediments to derive continental paleotemperatures. Only sediments which are under strong river influence should be considered acceptable for this purpose. In-situ production of brGDGTs in the marine environment does not have a strong influence on the BIT, since the concentration of brGDGTs is much lower than that of crenarchaeol. No obvious influence on the TEX_{68} paleothermometer by the riverine isoGDGTs is detected in marine SPM and sediments due to similar TEX_{86} values in the river and marine SPM and sediments.

ACKNOWLEDGEMENTS

We are grateful for the constructive comments of two anonymous reviewers. We also thank the crew of the R/V Knorr for their great services during the cruise, E. Montes and E. Goddard at the University of South Florida for sampling assistance while on cruise and the carbon analyses, and Dr. E.C. Hopmans and J. Ossebaar for analytical support at NIOZ. The research leading to these results has received funding from the European Research Council under the European Union's Seventh Framework Program (FP7/2007–2013)/ERC grant agreement No. [226600] (to J.S. Sinninghe Damsté) and from NSF-OCE-0823650 (to P. Baker).

REFERENCES

Aller R. C., Blair N. E., Xia Q. and Rude P. D. (1996) Remineralization rates, recycling, and storage of carbon in Amazon shelf sediments. *Cont. Shelf Res.* **16**, 753–786.

Antonov J. I., Seidov D., Boyer T. P., Locarnini R. A., Mishonov A. V., Garcia H. E., Baranova O. K., Zweng M. M. and Johnson D. R. (2010) World Ocean Atlas 2009, vol. 2: salinity. In *NOAA Atlas NESDIS 69* (ed. S. Levitus). Government Printing Office, Washington, DC, U.S., p. 184.

Ballantyne A. P., Greenwood D. R., Sinninghe Damsté J. S., Csank A. Z., Eberle J. J. and Rybczynski N. (2010) Significantly warmer Arctic surface temperatures during the Pliocene indicated by multiple independent proxies. *Geology* **38**, 603–606.

Bendle J. A., Weijers J. W. H., Maslin M. A., Sinninghe Damsté J. S., Schouten S., Hopmans E. C., Boot C. S. and Pancost R. D. (2010) Major changes in glacial and Holocene terrestrial temperatures and sources of organic carbon recorded in the Amazon fan by tetraether lipids. *Geochem. Geophys. Geosyst.* **11**, Q12007. http://dx.doi.org/10.1029/2010GC003308.

Blaga C. I., Reichart G.-J., Heiri O., Sjuijs A. and Sinninghe Damsté J. S. (2009) Tetraether membrane lipid distributions in water-column particulate matter and sediments: a study of 47 European lakes along a north–south transect. *J. Paleolimnol.* **41**, 523–540.

Blair N. E. and Aller R. C. (2012) The Fate of terrestrial organic carbon in the marine environment. *Annu. Rep. Mar. Sci.* **4**, 401–423.

Brochier-Armanet C., Boussau B., Gribaldo S. and Forterre P. (2008) Mesophilic crenarchaeota: proposal for a third archaeal phylum, the Thaumarchaeota. *Nat. Rev. Microbiol.* **6**, 245–252.

Conrad R., Klose M., Claus P. and Enrich-Prast A. (2010) Methanogenic pathway, ^{13}C isotope fractionation, and archaeal community composition in the sediment of two clear-water lakes of Amazonia. *Limnol. Oceanogr.* **55**(2), 689–702.

Callède J., Kosuth P., Loup J.-L. and GuimarãEs V. S. (2000) Discharge determination by acoustic doppler current profilers (ADCP): a moving bottom error correction method and its application on the River Amazon at Óbidos. *Hydrol. Sci. J.* **45**, 911–924.

Damuth J. E. and Flood R. D. (1985) Amazon Fan, Atlantic Ocean. In *Submarine Fans and Related Turbidite Sequences* (eds. A. H. Bouma, W. R. Normark and N. E. Barnes). Springer, New York, pp. 97–106.

Damuth E. J. and Kumar N. (1975) Amazon cone: morphology, sediments, age, and growth pattern. *Geol. Soc. Am. Bull.* **86**, 863–878.

Donders T. H., Weijers J. W. H., Munsterman D. K., Kloosterboer-van Hoeve M. L., Buckles L. K., Pancost R. D., Schouten S., Sinninghe Damsté J. S. and Brinkhuis H. (2009) Strong climate coupling of terrestrial and marine environments in the Miocene of northwest Europe. *Earth Planet. Sci. Lett.* **281**, 215–225.

Dunne T., Mertes L. A. K., Meade R. H., Richey J. E. and Forsberg B. R. (1998) Exchanges of sediment between the flood plain and channel of the Amazon River in Brazil. *Geol. Soc. Am. Bull.* **110**, 450–467.

Fawcett P. J., Werne J. P., Anderson R. S., Heikoop J. M., Brown E. T., Berke M. A., Smith S. J., Goff F., Donohoo-Hurley L., Cisneros-Dozal L. M., Schouten S., Sinninghe Damsté J. S., Huang Y., Toney J., Fessenden J., WoldeGabriel G., Atudorei V., Geissman J. W. and Allen C. D. (2011) Extended megadroughts in the southwestern United States during Pleistocene interglacials. *Nature* **470**, 518–521.

Fietz S., Martínez-Garcia A., Huguet C., Rueda G. and Rosell-Melé A. (2011) Constraints in the application of the Branched and Isoprenoid Tetraether index as a terrestrial input proxy. *J. Geophys. Res. Oceans* **116**, C10032. http://dx.doi.org/10.1029/2011JC007062.

Fietz S., Prahl F. G., Moraleda N. and Rosell-Melé A. (2013) Eolian transport of glycerol dialkyl glycerol tetraethers (GDGTs) off northwest Africa. *Org. Geochem.* **64**, 112–118.

Gibbs R. J. (1982) Currents on the shelf of north-eastern South America. *Coastal Shelf Sci.* **14**, 283–299.

Goulding M., Barthem R. and Ferreira E. (2003) *The Smithsonian Atlas of the Amazon*. Smithsonian Books, Washington, DC, p. 255.

Harvey H. R., Fallon R. D. and Patton J. S. (1986) The effect of organic-matter and oxygen on the degradation of bacterial-membrane lipids in marine-sediments. *Geochim. Cosmochim. Acta* **50**, 795–804.

Herfort L., Schouten S., Boon J. P., Woltering M., Baas M., Weiers J. W. H. and Sinninghe Damsté J. S. (2006) Characterization of transport and deposition of terrestrial organic matter in the southern North Sea using the BIT index. *Limnol. Oceanogr.* **51**, 2196–2205.

Hopmans E. C., Weijers J. W. H., Schefuβ E., Herfort L., Sinninghe Damsté J. S. and Schouten S. (2004) A novel proxy for terrestrial organic matter in sediments based on branched and isoprenoid tetraether lipids. *Earth Planet. Sci. Lett.* **224**, 107–116.

Hu J., Meyers P. A., Chen G., Peng P. and Yang Q. (2012) Archaeal and bacterial glycerol dialkyl glycerol tetraethers in sediments from the Eastern Lau Spreading Center, South Pacific Ocean. *Org. Geochem.* **43**, 162–167.

Huguet C., Hopmans E. C., Febo-Ayala W., Thompson D. H., Sinninghe Damsté J. S. and Schouten S. (2006) An improved method to determine the absolute abundance of glycerol dibiphytanyl glycerol tetraether lipids. *Org. Geochem.* **37**, 1036–1041.

Kim J.-H., Ludwig W., Schouten S., Kerherv P., Herfort L., Bonnin J. and Sinninghe Damsté J. S. (2007) Impact of flood events on the transport of terrestrial organic matter to the ocean: a study of the Têt River (SW France) using the BIT index. *Org. Geochem.* **38**, 1593–1606.

Kim J.-H., Van der Meer J., Schouten S., Helmke P., Willmott V., Sangiorgi F., Koç N., Hopmans E. C. and Sinninghe Damsté J. S. (2010) New indices and calibrations derived from the distribution of crenarchaeal isoprenoid tetraether lipids: implications for past sea surface temperature reconstructions. *Geochim. Cosmochim. Acta* **74**, 4639–4654.

Kim J.-H., Romero O. E., Lohmann G., Donner B., Laepple T., Haam E. and Sinninghe Damsté Jaap S. (2012a) Pronounced subsurface cooling of North Atlantic waters off Northwest Africa during Dansgaard-Oeschger interstadials. *Earth Planet. Sci. Lett.* **339–340**, 95–102.

Kim J.-H., Zell C., Moreira-Turcq P., Pérez M. A. P., Abril G., Mortillaro J.-M., Weijers J. W. H., Meziane T. and Sinninghe

Damsté (2012b) Tracing soil organic carbon in the lower Amazon River and its tributaries using GDGT distributions and bulk organic matter properties. *Geochim. Cosmochim. Acta* **90**, 163–180.

Kuehl S. A., DeMaster D. J. and Nittrouer C. A. (1986) Nature of sediment accumulation on the Amazon continental shelf. *Cont. Shelf Res.* **6**, 209–225.

Lengger S. K., Hopmans E. C., Reichart G.-J., Nierop K. G. J., Sinninghe Damsté J. S. and Schouten S. (2012) Intact polar and core glycerol dibiphytanyl glycerol tetraether lipids in the Arabian Sea oxygen minimum zone. Part II: Selective preservation and degradation in sediments and consequences for the TEX86. *Geochim. Cosmochim. Acta* **98**, 244–258.

Lentz S. J. and Limeburner R. (1995) The Amazon River plume during AMASSEDS: spatial characteristics and salinity variability. *J. Geophys. Res.* **100**, 2355–2375.

Liu X.-L., Leider A., Gillespie A., Gröger J., Versteegh G. J. M. and Hinrichs K.-U. (2010) Identification of polar lipid precursors of the ubiquitous branched GDGT orphan lipids in a peat bog in Northern Germany. *Org. Geochem.* **41**, 653–660.

Locarnini R. A., Mishonov A. V., Antonov J. I., Boyer T. P., Garcia H. E., Baranova O. K., Zweng M. M. and Johnson D. R. (2010) World Ocean Atlas 2009, vol. 1: temperature. In *NOAA Atlas NESDIS 68* (ed. S. Levitus). Government Printing Office, Washington, DC, U.S., p. 184.

Logemann J., Graue J., Köster J., Engelen B., Rullkötter J. and Cypionka H. (2011) A laboratory experiment of intact polar lipid degradation in sandy sediments. *Biogeosciences* **8**, 2547–2560.

Lorrain A., Savoye N., Chauvaud L., Paulet Y.-M. and Naulet N. (2003) Decarbonation and preservation method for the analysis of organic C and N contents and stable isotope ratios of low-carbonated suspended particulate material. *Anal. Chim. Acta* **491**, 125–133.

Meade R. H. (1994) Suspended sediments of the modern Amazon and Orinoco rivers. *Quat. Int.* **21**, 29–39.

Milliman J. D., Summerhayes C. P. and Barretto H. T. (1975) Quaternary sedimentation on the Amazon continental margin: a model. *Geol. Soc. Am. Bull.* **86**, 610.

Milliman J. D. and Meade R. H. (1983) World-wide delivery of river sediment to the oceans. *J. Geol.* **91**, 1–21.

Muller-Karger F. E., McClain C. R. and Richardson P. L. (1988) The dispersal of the Amazon's water. *Nature* **333**, 56–59.

Nittrouer C. A. and DeMaster D. J. (1986) Sedimentary processes on the Amazon continental shelf: past, present and future research. *Cont. Shelf Res.* **6**, 5–30.

Oba M., Sakata S. and Tsunogai U. (2006) Polar and neutral isopranyl glycerol ether lipids as biomarkers of archaea in near-surface sediments from the Nankai. *Org. Geochem.* **37**, 1643–1654.

Oppermann B. I., Michaelis W., Blumenberg M., Frerichs J., Schulz H. M., Schippers A., Beaubien S. E. and Krüger M. (2010) Soil microbial community changes as a result of long-term exposure to a natural CO_2 vent. *Geochim. Cosmochim. Acta* **74**, 2697–2716.

Pancost R. D. and Sinninghe Damsté J. S. (2003) Carbon isotopic compositions of prokaryotic lipids as tracers of carbon cycling in diverse settings. *Chem. Geol.* **195**, 29–58.

Peterse F., Kim J.-H., Schouten S., Klitgaard Kristensen D., Koç N. and Sinninghe Damsté J. S. (2009) Constraints on the application of the MBT–CBT palaeothermometer at high latitude environments (Svalbard, Norway). *Org. Geochem.* **40**, 692–699.

Peterse F., Hopmans E. C., Schouten S., Mets A., Rijpstra W. I. C. and Sinninghe Damsté J. S. (2011a) Identification and distribution of intact polar branched tetraether lipids in peat and soil. *Org. Geochem.* **42**, 1007–1015.

Peterse F., Prins M. A., Beets C. J., Troelstra S. R., Zheng H., Gu Z., Schouten S. and Sinninghe Damsté J. S. (2011b) Decoupled warming and monsoon precipitation in East Asia over the last deglaciation. *Earth Planet. Sci. Lett.* **301**, 256–264.

Peterse F., van der Meer J., Schouten S., Weijers J. W. H., Fierer N., Jackson R. B., Kim J.-H. and Sinninghe Damsté J. S. (2012) Revised calibration of the MBT–CBT paleotemperature proxy based on branched tetraether membrane lipids in surface soils. *Geochim. Cosmochim. Acta* **96**, 215–229.

Pitcher A., Hopmans E. C., Schouten S. and Sinninghe Damsté J. S. (2009) Separation of core and intact polar archaeal tetraether lipids using silica columns: insights into living and fossil biomass contributions. *Org. Geochem.* **40**, 12–19.

Pitcher A., Rychlik N., Hopmans E. C., Spieck E., Rijpstra W. I. C., Ossebaar J., Schouten S., Wagner M. and Sinninghe Damsté J. S. (2010) Crenarchaeol dominates the membrane lipids of Candidatus Nitrososphaera gargensis, a thermophilic Group I. 1b Archaeon. *ISME J.* **4**, 542–552.

Pitcher A., Hopmans E. C., Mosier A. C., Park S.-J., Rhee S.-K., Francis C. A., Schouten S. and Sinninghe Damsté J. S. (2011) Core and intact polar glycerol dibiphytanyl glycerol tetraether lipids of ammonia-oxidizing archaea enriched from marine and estuarine sediments. *Appl. Environ. Microbiol.* **77**, 3468–3477.

Powers L., Werne J. P., Vanderwoude A. J., Sinninghe Damsté J. S., Hopmans E. C. and Schouten S. (2010) Applicability and calibration of the TEX86 paleothermometer in lakes. *Org. Geochem.* **41**, 404–413.

Rueda G., Rosell-Melé A., Escala M., Gyllencreutz R. and Backman J. (2009) Comparison of instrumental and GDGT-based estimates of sea surface and air temperatures from the Skagerrak. *Org. Geochem.* **40**, 287–291.

Schouten S., Hopmans E. C., Pancost R. D. and Sinninghe Damsté J. S. (2000) Widespread occurrence of structurally diverse tetraether membrane lipids: evidence for the ubiquitous presence of low-temperature relatives of hyperthermophiles. *Proc. Natl. Acad. Sci.* **97**, 14421–14426.

Schouten S., Hopmans E. C., Schefuß E. and Sinninghe Damsté J. S. (2002) Distributional variations in marine crenarchaeotal membrane lipids: a new tool for reconstructing ancient sea water temperatures? *Earth Planet. Sci. Lett.* **204**, 265–274.

Schouten S., Huguet C., Hopmans E. C., Kienhuis M. V. M. and Sinninghe Damsté J. S. (2007) Analytical methodology for TEX86 paleothermometry by high-performance liquid chromatography/atmospheric pressure chemical ionization-mass spectrometry. *Anal. Chem.* **79**, 2940–2944.

Schouten S., Van der Meer M. T. J., Hopmans E. C. and Sinninghe Damsté J. S. (2008) "Lipids of marine archaea: patterns and provenance in the water column and sediments" by Turich et al. (2007). *Geochim. Cosmochim. Acta* **72**, 5342–5346.

Schouten S., Hopmans E. C. and Sinninghe Damsté J. S. (2013a) The organic geochemistry of glycerol dialkyl glycerol tetraether lipids: a review. *Org. Geochem.* **54**, 19–61.

Sinninghe Damsté J. S., Hopmans E. C., Pancost R. D., Schouten S. and Geenevasen J. A. J. (2000) Newly discovered non-isoprenoid glycerol dialkyl glycerol tetraether lipids in sediments. *Chem. Commun.*, 1683–1684.

Schouten S., Hopmans E. C. and Sinninghe Damsté J. S. (2013b) The organic geochemistry of glycerol dialkyl glycerol tetraether lipids: a review. *Org. Geochem.* **54**, 19–61.

Sinninghe Damsté J. S., Schouten S., Hopmans E. C., Van Duin A. C. T. and Geenevasen J. A. J. (2002) Crenarchaeol: the characteristic core glycerol dibiphytanyl glycerol tetraether membrane lipid of cosmopolitan pelagic crenarchaeota. *J. Lipid Res.* **43**, 1641–1651.

Sinninghe Damsté J. S., Ossebaar J., Abbas B., Schouten S. and Verschuren D. (2009) Fluxes and distribution of tetraether

lipids in an equatorial African lake: constraints on the application of the TEX86 palaeothermometer and BIT index in lacustrine settings. *Geochim. Cosmochim. Acta* **73**, 4232–4249.

Sinninghe Damsté J. S., Rijpstra W. I. C., Hopmans E. C., Weijers J. W. H., Foesel B. U., Overmann J. and Dedysh S. N. (2011) 13,16-Dimethyl octacosanedioic acid (iso-diabolic acid), a common membrane-spanning lipid of Acidobacteria subdivisions 1 and 3. *Appl. Environ. Microbiol.* **77**, 4147–4154.

Smith R. W., Bianchi T. S. and Li X. (2012) A re-evaluation of the use of branched GDGTs as terrestrial biomarkers: implications for the BIT Index. *Geochim. Cosmochim. Acta* **80**, 14–29.

Spang A., Hatzenpichler R., Brochier-Armanet C., Rattei T., Tischler P., Spieck Ev, Streit W., Stahl David A., Wagner M. and Schleper C. (2010) Distinct gene set in two different lineages of ammonia-oxidizing archaea supports the phylum Thaumarchaeota. *Trends Microbiol.* **18**, 331–340.

Strong D. J., Flecker R., Valdes P. J., Wilkinson I. P., Rees J. G., Zong Y. Q., Lloyd J. M., Garrett E. and Pancost R. D. (2012) Organic matter distribution in the modern sediments of the Pearl River estuary. *Org. Geochem.* **49**, 68–82.

Tyler J. J., Nederbragt A. J., Jones V. J. and Thurow J. W. (2010) Assessing past temperature and soil pH estimates from bacterial tetraether membrane lipids: evidence from the recent lake sediments of Lochnagar, Scotland. *J. Geophys. Res.* **115**. http://dx.doi.org/10.1029/2009JG001109.

Weijers J. W. H., Schouten S., Hopmans E. C., Geenevasen J. A. J., David O. R. P., Coleman J. M., Pancost R. D. and Sinninghe Damsté J. S. (2006a) Membrane lipids of mesophilic anaerobic bacteria thriving in peats have typical archaeal traits. *Environ. Microbiol.* **8**, 648–657.

Weijers J. W. H., Schouten S., Spaargaren O. C. and Sinninghe Damsté J. S. (2006b) Occurrence and distribution of tetraether membrane lipids in soils: implications for the use of the TEX86 proxy and the BIT index. *Org. Geochem.* **37**, 1680–1693.

Weijers J. W. H., Schefuβ E., Schouten S. and Sinninghe Damsté J. S. (2007a) Coupled thermal and hydrological evolution of tropical Africa over the last deglaciation. *Science* **315**, 1701–1704.

Weijers J. W. H., Schouten S., Van den Donker J. C., Hopmans E. C. and Sinninghe Damsté J. S. (2007b) Environmental controls on bacterial tetraether membrane lipid distribution in soils. *Geochim. Cosmochim. Acta* **71**, 703–713.

Weijers J. W. H., Panoto E., Van Bleijswijk J., Schouten S., Rijpstra W. I. C., Balk M., Stams A. J. M. and Sinninghe Damsté J. S. (2009a) Constraints on the biological source(s) of the orphan branched tetraether membrane lipids. *Geomicrobiol. J.* **26**, 402–414.

Weijers J. W. H., Schouten S., Schefuss E., Schneider R. R. and Sinninghe Damsté J. S. (2009b) Disentangling marine, soil and plant organic carbon contributions to continental margin sediments: a multi-proxy approach in a 20,000 year sediment record from the Congo deep-sea fan. *Geochim. Cosmochim. Acta* **73**, 119–132.

Weijers J. W. H., Bernhardt B., Peterse F., Werne J. P., Dungait J. A. J., Schouten S. and Sinninghe Damsté J. S. (2011) Absence of seasonal patterns in MBT–CBT indices in mid-latitude soils. *Geochim. Cosmochim. Acta* **75**, 3179–3190.

Wittmann H., von Blanckenburg F., Maurice L., Guyot J. L., Filizola N. and Kubik P. W. (2011) Sediment production and delivery in the Amazon River basin quantified by in situ-produced cosmogenic nuclides and recent river loads. *Geol. Soc. Am. Bull.* **123**, 934–950.

Xie S., Pancost R. D., Chen L., Evershed R. P., Yang H., Zhang K., Huang J. and Xu Y. (2012) Microbial lipid records of highly alkaline deposits and enhanced aridity associated with significant uplift of the Tibetan Plateau in the Late Miocene. *Geology* **40**, 291–294.

Zell C., Kim J.-H., Moreira-Turcq P., Abril G., Hopmans E. C., Bonnet M.-P., Lima Sobrinho R. and Sinninghe Damsté J. S. (2013a) Disentangling the origins of branched tetraether lipids and crenarchaeol in the lower Amazon River: implications for GDGT-based proxies. *Limnol. Oceanogr.* **58**, 343–353.

Zell C., Kim J.-H., Abril G., Sobrinho R. L., Dorhout D., Moreira-Turcq P. and Sinninghe Damsté J. S. (2013b) Impact of seasonal hydrological variation on the distributions of tetraether lipids along the Amazon River in the central Amazon basin: implications for the MBT/CBT paleothermometer and the BIT index. *Front. Microbiol.* **4**. http://dx.doi.org/10.3389/fmicb.2013.00228.

Zhang C. L., Wang J., Wei Y., Zhu C., Huang L. and Dong H. (2012) Production of branched tetraether lipids in the lower Pearl River and estuary: effects of extraction methods and impact on bGDGT proxies. *Front. Microbiol.* **2**. http://dx.doi.org/10.3389/fmicb.2011.00274.

Zhu C., Weijers J. W. H., Wagner T., Pan J. M., Chen J. F. and Pancost R. D. (2011) Sources and distributions of tetraether lipids in surface sediments across a large river-dominated continental margin. *Org. Geochem.* **42**, 376–386.

Zink K.-G., Vandergoes M. J., Mangelsdorf K., Dieffenbacher-Krall A. C. and Schwark L. (2010) Application of bacterial glycerol dialkyl glycerol tetraethers (GDGTs) to develop modern and past temperature estimates from New Zealand lakes. *Org. Geochem.* **41**, 1060–1066.

Associate editor: Thomas Wagner